

Dust evolution in protoplanetary disks

Nienke van der Marel and Paola Pinilla

Abstract Planet formation models rely on knowledge of the physical conditions and evolutionary processes in protoplanetary disks, in particular the grain size distribution and dust growth timescales. In theoretical models, several barriers exist that prevent grain growth to pebble sizes and beyond, such as the radial drift and fragmentation. Pressure bumps have been proposed to overcome such barriers. In the past decade ALMA has revealed observational evidence for the existence of such pressure bumps in the form of dust traps, such as dust rings, gaps, cavities and crescents through high-resolution millimeter continuum data originating from thermal dust emission of pebble-sized dust grains. These substructures may be related to young protoplanets, either as the starting point or the consequence of early planet formation. Furthermore, disk dust masses have been measured for complete samples of young stars in clusters, which provide initial conditions for the solid mass budget available for planet formation. However, observational biases exist in the selection of high-resolution ALMA observations and uncertainties exist in the derivation of the disk dust mass, which both may affect the observed trends. This chapter describes the latest insights in dust evolution and disk continuum observations. Specifically, disk populations and evolutionary trends are described, as well as the uncertainties therein, and compared with exoplanet demographics.

Nienke van der Marel

Leiden Observatory, Niels Bohrweg 2, 2333 CA Leiden, The Netherlands, e-mail: nmarel@strw.leidenuniv.nl

Paola Pinilla

Mullard Space Science Laboratory, University College London, Holmbury St Mary, Dorking, Surrey, RH5 6NT, UK e-mail: p.Pinilla@ucl.ac.uk

Introduction

Planets form in protoplanetary disks of gas and dust in the early stages of the disk, during or right after the formation of the protostar. The formation scenario is generally visualized as the coagulation of small dust grains into larger and larger particles through collisions. This process involves the growth from sub-micron sized dust particles up to 1000s of kilometer sized planets and planet cores, or more than 12 orders of magnitude in size and more than 36 orders of magnitude in mass within less than 10 Myr (Figure 1). The formation of the core may be followed by gas accretion, creating a gas giant, which must happen before the gas disk has dissipated. The mean gas disk lifetime has long been thought to be 2-3 Myr (Hernández et al. 2007), but recent work suggests that the mean lifetime may be as long as 5-10 Myr (Michel et al. 2021; Pfalzner et al. 2022). The key issue in understanding the planet formation process is thus primarily understanding the formation timescales of rocky cores through dust growth.

Various disk processes are responsible for both aid and hindrance of the efficiency of this coagulation, where the combined efficiencies and timescales of these processes have not been fully understood yet. One of the major complexities in this problem is that in protoplanetary disks only the smallest dust pebbles (micron-sized up to centimeter-pebble-sized) are observable, as larger boulders and planetesimals do not emit efficiently any more. Only the end product, the exoplanet population, becomes observable again, but all the steps in between remain mostly constrained by formation models, and by clues from remnants of the planet formation process in the Solar System. However, protoplanetary disk observations can provide answers as well through statistical studies and spatially resolved observations of substructures, which may show indirect evidence for early planet formation, as well as provide constraints on the initial conditions of the birth environments of planets.

The research field of protoplanetary disks has evolved tremendously in the past two decades, through new observational facilities in infrared and (sub)millimeter and developments in disk dynamics and dust evolution modeling. In particular the Atacama Large Millimeter/submillimeter Array (ALMA) and optical/infrared (OIR) instruments at 8m-class telescopes like VLT, Gemini and Subaru have provided a wealth of data in the form of spatially resolved images of dust and gas in disks, both in the early embedded stage where the disk is still surrounded by an envelope (also called Class 0 or Class I stage), the massive protoplanetary disk stage (Class II) and the evolved debris disk stage consisting of stars surrounded by Kuiper-belt equivalents. This chapter aims to summarize to most important insights in the study of dust in protoplanetary disks from the past decade and their implications for exoplanets and planet formation, as well as the open questions and issues that remain under debate. Observational constraints on the disk gas composition are described in the chapter ‘Chemistry During the Gas-Rich Stage of Planet Formation’.

This chapter is organized as follows. First, the main dust evolution processes are reviewed, including radial drift, trapping and transport, as well as challenges in dust evolution models. Second, an overview of observations of large-scale substructures in protoplanetary disks is presented, with most emphasis on (sub)millimeter obser-

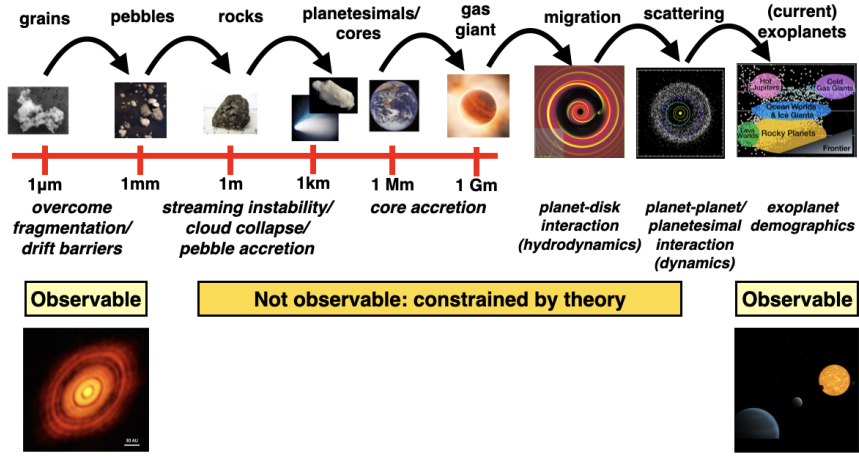


Fig. 1 Schematic of the growth from micron-sized grains to cores and planets

Observations with ALMA but some discussions on results from OIR imaging and VLTI results as well. In particular, the different types of substructures are discussed, including observational evidence for their role in the evolution of the disk and the biases in the detectability of substructures so far. Third, the main methods to derive disk dust masses and the uncertainties in this approach are reviewed, as well as the consequences for the solid mass budget available for planet formation. Observational constraints on grain sizes in disks are discussed as well. A discussion on trends in exoplanets with stellar mass and metallicity and possible similarities in disk demographic studies is included. The chapter finishes with a summary and an outlook to future facilities.

Dust Evolution in Protoplanetary Disks

Protoplanetary disks are the sub-product of angular momentum conservation in the star formation process, where the angular momentum of molecular clouds is much higher than the resulting protostars. As a consequence, the angular momentum is re-distributed in a rotating disk around the young star. In these disks, which are the birth sites of planets, the angular momentum and mass are transported by different physical mechanisms, such as the magneto-rotational instability (MRI, Pringle 1981), or a magnetohydrodynamical wind (e.g., Bai and Stone 2013), while the material is accreted onto the star.

The initial abundances of protoplanetary disks are thought to be similar to the interstellar medium, which means that most of the material is molecular gas ($\sim 99\%$ of the mass), while only $\sim 1\%$ is dust with an initial size of (sub-)micron-sized par-

ticles. These particles are the seeds for the formation of pebbles and planetesimals, which are the building blocks of planets.

The growth from interstellar dust particles to pebbles is a complex process that is regulated by the interaction of the dust with the gas. In this process, particles move in the disk due to different velocities, including: Brownian motion, settling, radial drift, and turbulence (e.g., Brauer et al. 2008; Birnstiel et al. 2010). How relevant each of these velocities are to the total velocity of particles depends on how well the particles are coupled to the gas, which is measured by the importance of the drag forces by comparing stopping time of the particles to the Keplerian frequency. This is quantified by the Stokes number, which is the stopping time normalized by the orbital timescale. While different drag regimes exist, dust particles in the gaseous disk typically fall in the Epstein drag regime, where the particle size is smaller than the mean free path of gas molecules. In the Epstein regime, the Stokes number is defined as

$$St = \frac{a\rho_s}{\Sigma_g} \frac{\pi}{2}, \quad (1)$$

where a is the grain size, ρ_s is the intrinsic volume density of the particles, and Σ_g is the gas surface density. Equation 1 is valid near or at the midplane of the disk. For particles with $St \ll 1$ the main source for the relative velocities is Brownian motion and settling, and these are usually lower than the threshold velocity for catastrophic collisions. Hence, these dust motions lead to grain growth (Birnstiel et al. 2016). When the Stokes number of particles increases and reach values near unity, the turbulent and drift motions become the dominant sources for their velocities, which can lead to destructive collisions or the loss of dust particles towards the star in timescales that are shorter than few thousands of years. The threshold velocity for catastrophic collisions or fragmentation velocity is one of the main unknown parameters in models of dust evolution. The models rely on laboratory experiments and numerical simulations for limits on this quantity. The fragmentation velocity depends on surface energy of the grains and therefore on the particle composition (e.g., Blum and Wurm 2000; Wada et al. 2011; Musiolik et al. 2016). Although water-ice particles are expected to be more sticky than silicates, recent laboratory experiments that reach conditions similar to those in the Universe (low density, pressure and temperature) have challenged this idea (Gundlach et al. 2018; Musiolik and Wurm 2019; Steinpilz et al. 2019). Currently, it is thought that the fragmentation velocity of particles has a value from few to tens of m s^{-1} .

The growth process to sub-micron sized particles to pebbles is accessible observationally, since different wavelengths can trace different dust size particles. For example, scattered light observations at the optical and near infrared trace the distribution of micron-sized particles located in the upper layers of the disk. On the other hand, pebbles which are located in the midplane of the disk can absorb the light of similar wavelength and re-emit the light. This process can also be affected by scattering, as discussed later on. However, observationally accessing the information of boulders and planetesimals in protoplanetary disks is very challenging because of their very low opacities. As a result, there is an observational gap between peb-

bles and planets, that can only be closed by connecting dust/planetesimal evolution models to exoplanets statistics.

The following sections present the most important processes of the first steps of planet formation, in particular radial drift and its connection with observations. In this topic, a brief overview of the origin of substructures in disks is presented. This section ends with the current challenges in this field.

Dust Radial Drift

Depending on their Stokes number, particles experience different velocities. One of the main sources for dust velocities with particles with Stokes number near unity is radial drift. The drift velocity of particles originates from the sub-Keplerian azimuthal gas velocity in a disk where pressure decreases monotonically with radius. The total drift velocity of dust particles in protoplanetary disks is given by (Weidenschilling 1977):

$$v_{\text{drift}}(\text{St}, M_*, L_*) = \frac{1}{\text{St}^{-1} + \text{St}} \frac{\partial_r P(M_*, L_*)}{\rho(M_*, L_*) \Omega(M_*)}. \quad (2)$$

There is a dependency of v_{drift} on the stellar mass and luminosity that makes radial drift to be more efficient around low-mass stars and for stars more massive than $> 2.5 M_\odot$ (Pinilla et al. 2013, 2022; Zhu et al. 2018).

In Eq. 2 ρ is the disk gas volume density, which in hydrostatic balance and in a vertically isothermal disk is given by

$$\rho = \rho_0(M_*, L_*) \exp\left(\frac{-z^2}{2h^2(M_*, L_*)}\right), \quad (3)$$

where ρ_0 is the midplane density, h is the disk scale height, and P is the isothermal pressure, each of them given by

$$\rho_0 = \frac{\Sigma_g(M_*)}{\sqrt{2\pi}h(M_*, L_*)} \quad (4)$$

$$h(M_*, L_*) = \frac{c_s(L_*)}{\Omega(M_*)} \quad (5)$$

$$P = \rho(M_*, L_*) c_s^2(L_*), \quad (6)$$

respectively. The assumption that Σ_g depends on the stellar mass comes from assuming that the total disk mass scales with the stellar mass, supported by observations as described later. The sound speed (c_s) is given by:

$$c_s^2 = \frac{\sigma_{\text{SB}} T_{\text{disk}}(L_*)}{\mu m_p}, \quad (7)$$

with σ_{SB} , μ , and m_p the Stefan-Boltzmann constant, the mean molecular mass, and the proton mass, respectively. When assuming a disk temperature (T_{disk}) of a passive disk, there is a dependency between the disk temperature and stellar luminosity as (Kenyon and Hartmann 1987):

$$T(r, L_\star) = T_\star \left(\frac{R_\star}{r} \right)^{1/2} \phi_{\text{inc}}^{1/4} = \left(\frac{L_\star \phi_{\text{inc}}}{4\pi\sigma_{\text{SB}} r^2} \right)^{1/4}, \quad (8)$$

where R_\star and T_\star are the stellar radius and temperature, respectively, and ϕ_{inc} is the incident angle, which usually is a very small quantity.

These dependencies on stellar mass and luminosity, leaves to $v_{\text{drift}} \propto L_\star^{1/4} / \sqrt{M_\star}$. The left panel of Fig. 2 shows the absolute value of the drift velocity when $\text{St}=1$ as a function of time around stars with different masses, when assuming evolutionary tracks from Dotter et al. (2008) up to 30 Myr of $0.1\text{--}5 M_\odot$ stars. The drift velocities for particles with $\text{St}=1$ are pretty high, between $\sim 5000\text{--}8000 \text{cm s}^{-1}$, implying that grains with such a Stokes number will be quickly lost towards the star, for example at one astronomical unit, they will drift in less than 100 yr. This is the origin of the well-known *radial drift barrier*, which is due to high radial drift velocities that can lead to the lost of particles onto the star, or to the fragmentation of grains when they collide at these high drift velocities.

The drift barrier occurs when growth is limited by radial drift and is given by

$$a_{\text{drift}} = \frac{2\Sigma_d v_K^2}{\pi\rho_s c_s^2} \left| \frac{d \ln P}{d \ln r} \right|^{-1}, \quad (9)$$

Fragmentation due to turbulent velocities also can limit the growth of dust particles. Turbulence induces dust motion that depends on the dust particle size, this motion for example diffuse particles from dust particle concentrations as discussed later. Assuming that the disk turbulence is described by an effective viscosity, the well-known α -parameter (Shakura and Sunyaev 1973), and assuming that particles stick in collisions below a given fragmentation speed v_{frag} , the fragmentation limit is

$$a_{\text{frag}} = \frac{2}{3\pi} \frac{\Sigma_g}{\rho_s \alpha} \frac{v_{\text{frag}}^2}{c_s^2}. \quad (10)$$

The disk viscosity parameter α remains one of the most unknown quantities in models of planet formation. It is usually assumed constant throughout the disk. However, its value depends on the dust properties and its abundance, the magnetic field strength and its configuration, the gas and dust chemistry, and the various ionization sources (Delage et al. 2022; Lesur et al. 2022), whereas many of these properties cannot be constrained from disk observations. Theoretical models predict that when the disk is now well ionized, the disk viscosity can be low, which usually happens in the dense inner regions at the midplane. This region, known as the dead zone, is expected to have a lower effective viscosity than the rest of the disk.

Using typical disk and stellar parameters, the maximum grain size is set by fragmentation in the first ~ 20 au (e.g. Birnstiel et al. 2016, Figure 4), with values between few centimetres to few millimetres, while in the outer disk is limited by drift with values from few millimetres to hundreds of microns.

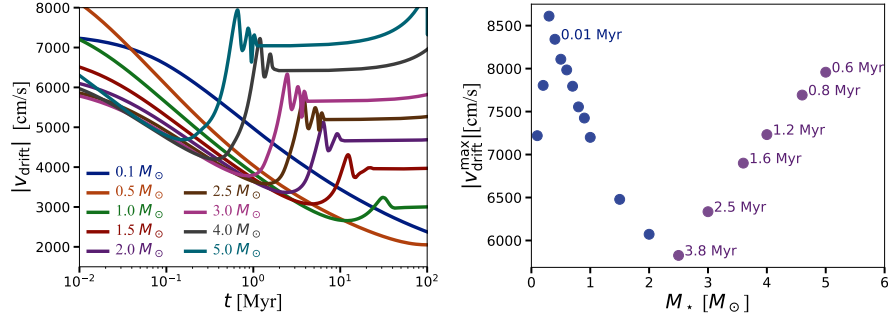


Fig. 2 *Left*: absolute value of the drift velocity when $St=1$ as a function of time around stars with different masses, when assuming evolutionary tracks from Dotter et al. (2008) up to 30 Myr of 0.1 – $5 M_{\odot}$ stars in the H-R diagram (adapted from Pinilla et al. 2022). *Right*: absolute value of the drift velocity when $St=1$ as a function of stellar mass. The values are taken at 0.01 Myr for all the stars with a mass $< 2.5 M_{\odot}$, while for more massive stars the drift velocity value is taken when it is maximum and this time is indicated for each point.

Dependency of radial drift with stellar mass

For different stellar masses, the maximum drift velocity in the left panel of Fig. 2 is taken and plotted against the stellar mass in the right panel of Fig. 2. For stars with a mass $< 2.5 M_{\odot}$, this value is taken at early times (0.01 Myr) when drift has its highest values, and for more massive stars, the time when the drift velocity is maximum, which is displayed. This figure shows the binomial behaviour of the radial drift. Specifically, for low-mass stars (0.1 – $0.5 M_{\odot}$) the drift velocity is higher than for a Solar-mass star throughout the disk lifetime. While for stars more massive than $2.5 M_{\odot}$, the drift velocities are lower at early times and sharply increase when the stellar luminosity also increases and this happens within the disk lifetime (< 5 – 10 Myr).

This interesting dependency of radial drift on stellar properties may explain different observational aspects of protoplanetary disks around different stellar masses. An example is the lack of disk detections around disks around stellar objects more massive than $2.5 M_{\odot}$ at ages older than 3 – 4 Myr (Benisty et al. 2022). In addition, this suggests that if pebbles are present in disks around low-mass stars, whichever physical process halting the drift should be more efficient around such stellar objects (Pinilla et al. 2013).

Solution to the Radial Drift Barrier and Origins of Substructures

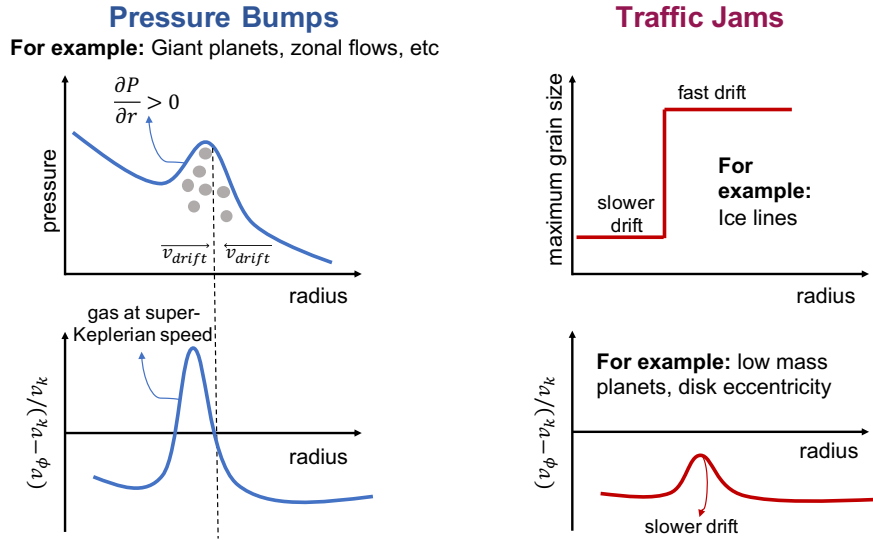


Fig. 3 Sketch to compare pressure bumps vs. traffic jams. In pressure bumps, the gas azimuthal velocity is positive where the pressure gradient is positive and as a result dust particles drift outwards, while they drift inwards in the rest of the disk where the pressure gradient is negative (Eq. 9). Traffic jams have different origins in disks. For example, when there are variations of the maximum grain size as expected near ice-lines of the main volatiles in disks. In the locations where the particle size is higher, particles drift faster due to their higher Stokes number and vice versa. Other possibilities of traffic jams happen when there is a perturbation in azimuthal gas velocity that makes particles to slow down their drift without the gas moving super-Keplerian (i.e. without a pressure bump).

There are two main solutions to reduce or totally stop the radial drift of particles in protoplanetary disks. One is to increase the cross-section of the particles, such that their Stokes number is low while they are still large (e.g., Kataoka et al. 2013). This will imply very fluffy aggregates that can be compressed by gas pressure and/or self-gravity of the aggregates. In this scenario, the compression processes need to be fast enough to avoid the drift barrier. The other alternative that has gained a lot of attention in the last decade is the presence of pressure bumps or traffic jams in protoplanetary disks.

In pressure bumps, there is a region where the pressure gradient is positive and as a consequence the particles drift outwards (Eq. 2). In the pressure maximum, the drift velocity of particles is zero. Dust evolution models of particle traps or dust traps have shown that the efficiency of trapping depends on the dust diffusion (or disk viscosity) and the pressure gradient. In a pressure bump, the disk viscosity sets the maximum grain size, and hence the Stokes number of the particles that

are trapped. Particles are efficiently trapped when $St \gtrsim \alpha$, otherwise radial diffusion makes particles escape the bump and trapping is inefficient (e.g., Pinilla et al. 2012a; de Juan Ovelar et al. 2016).

Some examples of particle traps are when a planet (usually more massive than Neptune) opens a planetary gap in the gas surface density that results in a pressure bump at the outer edge of the gap (e.g., Zhu et al. 2011; Gonzalez et al. 2012; Dong et al. 2015b; Zhang et al. 2018); variations of the disk magnetic field that leads to overdensities in the disk that result in pressure bumps as well (the well-known zonal flows, Uribe et al. 2011; Flock et al. 2015); or at the edge of a cavity formed by photoevaporation by the central star (e.g., Alexander et al. 2006; Owen et al. 2010; Picogna et al. 2019). In the recent review by Bae et al. (2022a), there is an extensive discussion about the potential origins of pressure bumps in disks.

In traffic jams, the radial (or azimuthal) drift of particles is reduced by different mechanisms, without the presence of pressure bumps. For example, it is thought that near ice-lines of main volatiles, particles change their composition and hence their capability to stick. For instance, inside the water ice-line where grains are mostly silicates, fragmentation due to collisions is efficient in these regions. As a consequence, the maximum grain size is reduced (Eq. 10 when v_{frag} is lower). As a consequence of the maximum grain size reduction, particles experience lower radial drift due to their low Stokes number (Eq. 2 and Eq. 1). How the maximum fragmentation velocity changes for different grain composition is still an open question. Pinilla et al. (2017) performed numerical simulation of dust evolution in the presence of one, two, or three ice-lines affecting the dust growth and dynamics, and produced observational predictions of the gaps and rings in disks.

Other alternatives for dust traffic jams in disks are when a low-mass planet is embedded in the disk or when the disk is eccentric. In the first case, a low mass planet that does not open a gap would nevertheless affect the azimuthal velocity of the gas, decreasing the drift velocity near the planet location (Fig. 3, e.g., Rosotti et al. 2016). These traffic jams can create also multiple rings and gaps that are observable with telescopes like ALMA.

Pressure bumps and traffic jams produced by different physical mechanisms can explain the structures observed in protoplanetary disks. Figure 4 shows examples of dust density distributions after $\sim 1 - 1.5$ Myr of evolution of dust evolution models performed with *Dustpy* (Stammler and Birnstiel 2022). These models include the dynamics and different growth processes (sticking, fragmentation, and erosion) of particles. The results from Figure 4 show:

- A Neptune-type planet embedded in the disk around 30 au. In this case, it is possible to see the dust trapping at the edge of the planetary gap. The more massive the planet is, a deeper and wider gap is created when assuming the same disk viscosity and thermodynamical properties. When the planet reaches a mass of $\sim 1 M_{\text{Jup}}$, it can open a very deep and wide gap in the distribution of pebbles, resembling properties of so-called transition disks (e.g., Zhu et al. 2011; Pinilla et al. 2012a).
- An artificial ice-line located at 20 au. In this simulation, the fragmentation velocity changes at 20 au from 1 inside to 10 m s^{-1} outside 20 au. Because dust

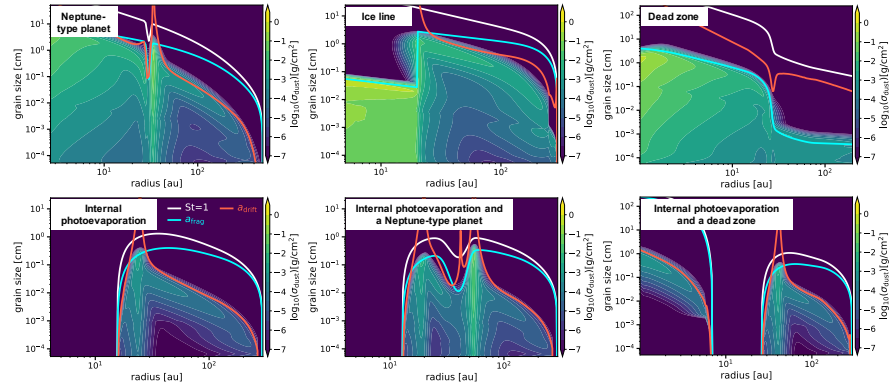


Fig. 4 Dust density distribution from dust evolution models after $\sim 1 - 1.5$ Myr of evolution for all the cases. From left-top panel are the models of: a Neptune-type planet (pressure bump); an ice-line (traffic jam) artificially set at 20 au where the fragmentation velocity changes from 1 inside to 10 m s^{-1} outside 20 au (Gárate et al. 2020); dead zone (traffic jam, models from Delage et al. 2023); internal photoevaporation (pressure bump) models from Garate et al. (submitted); and combinations of models of internal photoevaporation with either a Neptune-type planet or a dead zone Gárate et al. (2021) and submitted. The solid white line represents a Stokes number of unity (which is proportional to the gas surface density), while cyan and red show the fragmentation (Eq. 10) and drift (Eq. 9) barrier, respectively.

particles reduce their size and their Stokes number near this location, they slow down their drift. These density distributions can lead to clear substructures in the disk (Banzatti et al. 2015; Pinilla et al. 2017; Gárate et al. 2020).

- A dead zone which extends up to ~ 20 au. In this case there are variations of the disk viscosity that allow dust particles to grow larger inside 20 au (opposite to the case of the ice-line). Dust particles in the outer disk experience a reduction of their radial drift. Models are taken from Delage et al. (2023), where there is no self-consistent evolution of gas and dust yet, hence there is no trapping, but a traffic jam effect.
- Internal photoevaporation alone or in combination with an Neptune-type planet or a dead zone. Photoevaporation by the irradiation of the central star can open a very deep gap and particles are trapped at the edge of that gap. If a Neptune-type planet is embedded in the disk, there can be multiple regions of trapping at Myr timescales (Garate et al., submitted). In the case of internal photoevaporation combined with a dead zone, a wide gap is formed in the distribution of pebbles, while keeping an inner disk and averaged accretion rates as observed in transition disks (Gárate et al. 2021).

Although planet-disk interaction remains as one of the most used scenarios to explain observed substructures (see next section), other scenarios cannot be excluded until the planets are confirmed.

Dust Settling in Disks

From micron to sub-millimeter sized dust grains, settling is an important source for the velocity of the dust and their collisions. The settling velocity of grains is given by the balance of the gas drag force, vertical gravitational force, and the vertical stirring (or vertical turbulence) of particles. Large particles settle faster to the midplane due to gravity, which are also less affected by vertical stirring. The particle scale height h_d for a grain with a given Stokes number is (Youdin and Lithwick 2007; Birnstiel et al. 2010)

$$h_d(St) = h \times \min \left(1, \sqrt{\frac{\alpha}{\min(St, 1/2)(1 + St^2)}} \right). \quad (11)$$

Comparing optical and near-infrared observations that trace the distribution of the micron-sized particles and millimeter observations that trace the large particles that are subject to dust settling, Villenave et al. (2020, 2022, 2023) provided constraints on the level of vertical turbulence, which in most cases is quite moderate, with α as low as $10^{-5} - 10^{-4}$. Furthermore, high degrees of settling can enhance *grain growth* due to the locally high dust concentration.

Current challenges in dust evolution models

There are several physical processes that can affect dust evolution and that remain unconstrained from observations. For example, the disk temperature is a fundamental quantity of disks, and it can affect different properties, such as the disk composition and locations of ice lines of main volatiles in protoplanetary disks, hence where structures potentially formed by ice-lines are expected.

The fragmentation velocity for dust particles for different dust compositions remain still an open question. Most of the laboratory experiments of dust collisions do not have yet the temperatures and pressures that are expected in the disk midplane, and hence it remains unknown the sticky properties of particles with different compositions. This parameter has a large impact in the maximum grain size that particles can reach through collisional growth (Eq. 10)

In addition, the disk viscosity and turbulence are generally unknown in disks, and it directly affects the dust settling and growth. From observations of edge-on disks, the comparison of the distribution of micron-sized and millimeter-sized particles can provide insights about the vertical disk turbulence (Eq. 11), which in most cases suggest that disk turbulence is low. Other alternatives to obtain the disk turbulence is to measure the non-thermal broadening of molecular lines due to turbulence (e.g., Flaherty et al. 2015, 2020), and to measure the radial width of the sub-structures in disks (which are expected to be very narrow in the absence of turbulence that diffuse the dust particles inside these regions, see Dullemond et al. 2018; Rosotti

et al. 2019). Most of these observations suggest that the typical α in protoplanetary disks is rather low (see Rosotti 2023, for a review).

If disk viscosity is low, the question remains what is the main mechanism that drives the angular momentum transport and the evolution of protoplanetary disks. Knowing how the gas evolves in disks is fundamental to understand the dynamical behaviour of the particles. In fact, the gas disk mass and its distributions are poorly constrained from observations, but are crucial for determining the coupling of dust particles onto the gaseous disk.

Disk Observations

Large-scale Substructures in Protoplanetary Disks

The previous section has demonstrated that dust traps are expected to be present in disks to halt radial drift and enable grain growth. Such dust traps would appear as substructures in millimeter dust continuum images. High-resolution observations have revealed numerous substructures in the (sub)millimeter and optical/infrared images of protoplanetary disks, in particular in the ALMA continuum emission tracing thermal dust emission at wavelengths between 0.5 and 3 mm, where the 1.3 and 0.85 mm (230 and 345 GHz or ALMA Band 6 and 7) wavelengths are used most commonly (Andrews 2020). Dust disks in nearby star forming regions at 100-200 pc range in size from less than 10 to more than 100 au and their integrated continuum flux ranges from ~ 1 -100 mJy at 1.3 mm, which can be spatially resolved by ALMA in minutes. Substructures are seen in the form of e.g. rings, gaps, cavities, crescents, shadows and spiral arms, in clear contrast with the previously common assumption of smooth protoplanetary disks. Whereas the first large scale substructures were already seen in the pre-ALMA years in transition disks with large inner cavities (Brown et al. 2008, 2009; Andrews et al. 2011), the HL Tau disk that was observed at $\sim 0.04''$ spatial resolution (~ 6 au at 140 pc) as part of the ALMA Long Baseline Science Verification campaign (ALMA Partnership et al. 2015) revolutionized the field revealing multiple narrow rings and gaps. This was followed by numerous other high-resolution ALMA studies of disks, most noticeably the DSHARP ALMA Large Program, which targeted 20 of the brightest protoplanetary disks at $0.04''$ resolution, revealing rings, gaps, crescents (asymmetries) and spiral arms at scales from a few to a few tens of au (Andrews et al. 2018, and Figure 5). The distinction between a cavity and a gap (see Figure 5) is mostly historical, as cavities could already be identified through a deficit of infrared emission in the Spectral Energy Distribution (SED) and through imaging with pre-ALMA submillimeter interferometry (Espaillat et al. 2014) whereas gaps leave no signature in the SED and can only be revealed through high-resolution imaging. In the context of this chapter, the definition of a cavity is thus an inner dust gap that is >20 au in size with little

or no millimeter-dust inside following conventions in disk literature, whereas a dust gap is located in between narrow dust rings throughout the disk.

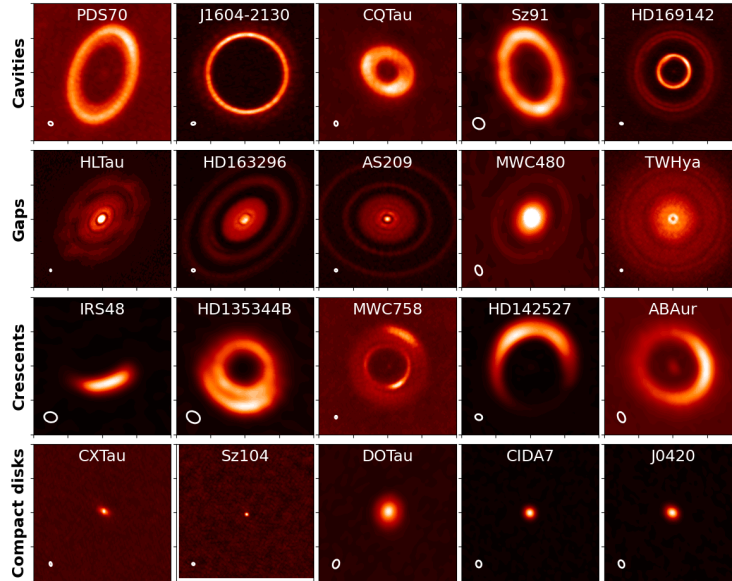


Fig. 5 ALMA continuum gallery of examples of dust structures in protoplanetary disks, categorized in disks with inner cavities, gaps, crescents and compact disks. The beam size is indicated in the lower left corner. Images are $2'' \times 2''$ in size, except for HD142527 and AB Aur, which have been zoomed out to $4'' \times 4''$ as their angular size is larger. Individual disks: PDS70 (Benisty et al. 2021), J1604-2130 (Stadler et al. 2023), CQ Tau (Ubeira Gabellini et al. 2019), Sz91 (Maucó et al. 2020), HD169142 (Pérez et al. 2019), HL Tau (ALMA Partnership et al. 2015), HD163296 (Andrews et al. 2018), AS209 (Andrews et al. 2018), MWC480 (Liu et al. 2019), TW Hya (Andrews et al. 2016), IRS48 (van der Marel et al. 2016), HD142527 (Casassus et al. 2015), AB Aur (van der Marel et al. 2021a), MWC758 (Dong et al. 2019), CX Tau (Facchini et al. 2019), Sz104 (van der Marel et al. 2022), DO Tau (Long et al. 2019), CIDA 7 (Kurtovic et al. 2021), J0420 (Kurtovic et al. 2021).

Substructures are thought to be connected with planet formation, but it is currently not yet clear whether they are the start or consequence of young protoplanets in the disk, or both. It is also unknown if all substructures, even for the same morphology, are caused by the same phenomenon, or whether this varies from disk to disk or perhaps per evolutionary stage. Rings, gaps and cavities are often associated with planet-disk interactions, as (growing) protoplanets will carve a gap in the

disk along their orbit (Artymowicz and Lubow 1996), where the depth and width of the gap depend on the planet mass and disk viscosity (e.g. Fung and Chiang 2016; Zhang et al. 2018): these observable parameters are thus key in connecting them with planet-disk interaction models. Although a minimum planet mass is required to create a dust gap, also called the pebble isolation mass, which is generally above a Neptune mass (Lambrechts et al. 2014; Rosotti et al. 2016), its value depends strongly on the assumed disk viscosity (Ataiee et al. 2018). On the other hand, if dust rings are the start of planet formation in dust traps (see previous section), other mechanisms not invoking planets may in fact be responsible for them, such as ice-lines, photoevaporation and numerous magneto-hydrodynamic (MHD) and other disk instabilities (see previous section and Bae et al. 2022a; Lesur et al. 2022, for an overview). In that case, local dust concentrations facilitate the formation of planetesimals and ultimately planets (Youdin and Goodman 2005; Johansen et al. 2007) rather than being caused by them. Whereas ice-lines initially appeared to be promising explanations for dust rings (Zhang et al. 2016), later studies showed that this could at least not be a universal explanation as ring radii did not correlate with ice-line radii in larger samples of disks (Huang et al. 2018; Long et al. 2018; van der Marel et al. 2019). However, temperature variations in the disk can be caused by different physical processes and instabilities (Owen 2020). MHD instabilities remain challenging to test observationally, and may only be confirmed by statistical arguments.

A proper test on the origin of gaps would be the direct detection of protoplanets in disks, but this remains observationally challenging with current instruments. Protoplanets have been firmly detected in three disks so far through direct imaging: PDS 70 (Keppler et al. 2018; Haffert et al. 2019), AB Aur (Currie et al. 2022) and HD 169142 (Hammond et al. 2023), as well as upper limit constraints in various other systems (e.g. Asensio-Torres et al. 2021; van der Marel et al. 2021a). Models of dust evolution and planet-disk interaction have demonstrated that inferring the planet mass from the morphology of the substructures is complicated and degenerate, because the shape of the substructures depends on different disk parameters (Bae et al. 2018). Indirect signs of the presence of protoplanets in gaps have been found in numerous disks as well, for example through deep gas cavities (e.g. van der Marel et al. 2016), non-Keplerian kinematics in CO line cubes (e.g. Pinte et al. 2018), pressure gradients (Teague et al. 2018), circumplanetary disks (Benisty et al. 2021; Bae et al. 2022b), localized shock emission (Booth et al. 2023) and spiral arms and shadows in scattered light images (e.g. Benisty et al. 2022, for an overview). Together with this indirect evidence, protoplanets seem to be a realistic explanation for at least the large scale gaps and cavities in disks, although other explanations (see previous section) cannot be excluded at this point for most systems. However, as dust concentrations are initially required to start the planet formation process, the chicken-and-egg problem of dust substructures remains.

Other than dust rings and gaps, other types of substructures have been observed regularly in disks as well even at lower resolution of 0.15-0.25", in particular crescents (asymmetries) and spiral arms, both in (sub)millimeter and scattered light images. Crescents have been detected along millimeter dust rings in various disks,

in a range of contrast values from 1.5-2 up to more than 100 (Pérez et al. 2014; Pinilla et al. 2014; van der Marel et al. 2021a). The first crescent disk, Oph IRS 48, provided robust observational evidence for the presence of dust trapping in disks (see previous section), by comparison of the distribution of the millimeter dust and gas and small dust grains (van der Marel et al. 2013). Crescents are also found in secondary rings (Cazzoletti et al. 2018) or as clumps in part of the ring (Pérez et al. 2018). Crescents are thought to be azimuthal variants of the radial dust traps discussed above, possibly due to Rossby Wave Instability leading to long-lived vortices (Barge and Sommeria 1995; Klahr and Henning 1997) or eccentric disks due to massive companions (Ataiee et al. 2013; Ragusa et al. 2017). Multi-wavelength observations tracing different grain sizes show different azimuthal widths (Pinilla et al. 2015; van der Marel et al. 2015; Casassus et al. 2015) and shifts in peak positions (Cazzoletti et al. 2018), consistent with modeling predictions (Birnstiel et al. 2013; Baruteau and Zhu 2016). van der Marel et al. (2021a) has proposed that mm-dust asymmetries only become visible at mm-wavelengths when dust rings are located at radii with low gas surface density (i.e. far out in the disk or in disks with low gas mass) to explain the diversity of crescents in disks but this remains to be proven with larger samples and better estimates of the gas surface densities in disks. Overall the sample of crescents in disks is rather small, with an occurrence less than 10%, which makes it difficult to address their nature w.r.t. axisymmetric dust rings.

Second, spiral arms have been detected in both scattered light (e.g. Benisty et al. 2022) and in millimeter emission (Pérez et al. 2016; Huang et al. 2018), and differences in appearance between the two wavelengths have been related to scale height (Juhász et al. 2015; Rosotti et al. 2019), whereas the origin has been interpreted as either spiral density waves triggered by companions (Dong et al. 2015a) or gravitational instabilities (Kratte and Lodato 2016), returning to the question in the beginning of this section: are substructures the result or start of planet formation?

Substructures in molecular line emission, in particular CO isotopologues, have been detected as well with ALMA, in some cases connected with the observed dust substructures. Disks with large inner dust cavities >30 au often show gas cavities in ^{13}CO and C^{18}O with radii that are 1-2 times smaller than their dust counter parts (e.g. van der Marel et al. 2016; Dong et al. 2017; Ubeira Gabellini et al. 2019), consistent with a planet gap model where dust is trapped at the outer edge of a gas gap (Pinilla et al. 2012b; Facchini et al. 2018). On the other hand, the narrow gaps of <10 au width remain mostly undetected in CO line emission, due to a combination of spatial resolution and temperature changes inside a dust gap (Isella et al. 2016; van der Marel et al. 2019; Rab et al. 2020). Radial substructure has been detected in images of other molecules in gapped disks, e.g. in the MAPS ALMA Large Program survey (Öberg et al. 2021), but without a clear correlation to the dust substructure (Law et al. 2021; Jiang et al. 2022), suggesting other physical mechanisms contribute to their gas abundance and excitation. Ice-lines and dust transport may play an important role in setting the molecular substructure, as molecules like N_2H^+ only become abundant when CO is frozen out, resulting in outer N_2H^+ rings (Qi et al. 2013, 2019), and ice-produced molecules like CH_3OH have been detected in disks with significant amount of warm dust at temperatures >100 K where these

molecules sublimate (Booth et al. 2021; van der Marel et al. 2021b). Furthermore, CO emission has revealed spiral structures in several disks after subtraction of the rotating disk component (Christiaens et al. 2014; Tang et al. 2017; Teague et al. 2019) similar to the scattered light images. Finally, CO line cubes show a range of non-Keplerian substructures which are thought to be linked to forming protoplanets as well, such as velocity kinks, warps, streamers and circumplanetary disks, which are not further discussed here, but are reviewed in detail by Pinte et al. (2022).

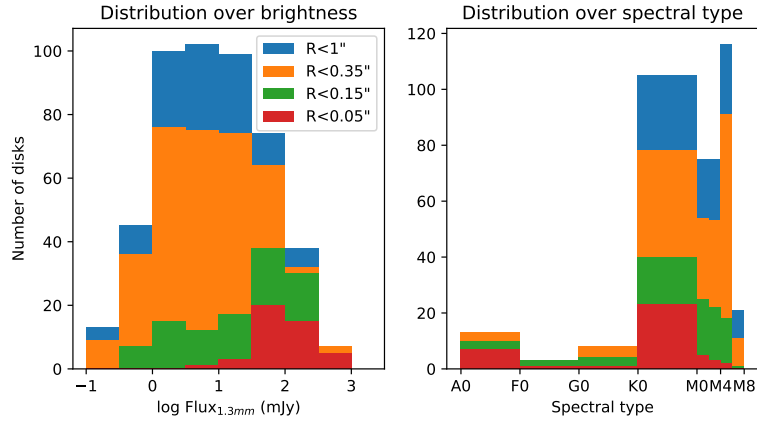


Fig. 6 The distribution of the observed angular resolution of protoplanetary disks imaged with ALMA, using the data from van der Marel and Mulders (2021) from the Taurus, Lupus, Ophiuchus, Chamaeleon and Upper Sco regions as well as isolated Herbig stars. In the left plot the distribution is shown w.r.t. the integrated flux, in the right plot w.r.t. spectral type. For clarity, the M-dwarfs are grouped per 2 subtypes. This plot demonstrates that high-resolution ALMA observations are relatively biased towards the brightest disks and the earliest spectral types, even though such disks are rare in the overall distribution.

Observational Biases

By today, it appears that almost any disk that is observed at sufficiently high angular resolution reveals some kind of substructure, but one has to be mindful of strong selection biases when drawing such conclusions. As the emission scales with the dust disk size (e.g. Tripathi et al. 2017), the most extended disks are also the brightest, and therefore the most often selected for high-resolution observations, which naturally results in a higher detectability of substructures (Bae et al. 2022a). Furthermore, the observed disk dust mass (see later discussion) scales with the stellar mass (e.g. Ansdell et al. 2016, 2017) and as the calculated dust mass is proportional to the integrated flux, the brightest disks are most commonly found around higher mass stars, introducing another bias. Whereas the prevalence of substructures on

first sight appears to be inconsistent with the occurrence rates of giant exoplanets, biases have to be considered before drawing such conclusions. In particular, the shape of the initial mass function (IMF) which peaks around mid-M or subsolar mass stars, and its corresponding coverage in high-resolution ALMA studies, directly reveals the biases that still trouble observational disk studies (see Figure 6). This figure also shows the bias towards brighter protoplanetary disks, making it clear that fainter, smaller disks are mostly unresolved in current ALMA observations at low spatial resolution, lacking any information on possible substructures. Disk populations and the attempts to correct for these biases are discussed at the end of this chapter.

Evolutionary Stages

Substructures in disks have been studied extensively in the protoplanetary disk or Class II stage at disks of 1-10 Myr as described in the previous section, but are also detected in the earlier, embedded disk stage. This stage is essentially defined as the time before the envelope from which the star and disk have formed has fully dissipated, in the first Myr of the lifetime of the disk. Given the chicken-and-egg problem of dust substructures and planet formation described in the beginning of this section, it is a natural question whether substructures are already present in the embedded stage, and if so, if they have a similar nature and origin as their counterparts in the Class II stage. If this is the case and proven to be caused by growing protoplanets, this sets firm constraints on the time available to form planet cores that are massive enough to carve gaps: such cores would have to form in less than 1 Myr, which is challenging for current planet formation models. On the other hand, if substructures are not present or clearly of a different nature, this would imply that other mechanisms like MHD instabilities or gravitational instabilities create initial dust concentrations, which result in protoplanets that carve the gaps and dust rings that are detected in the protoplanetary disk stage.

ALMA observations have already revealed substructures in younger disks. In fact, the first highly resolved disk HL Tau is a Class I disk, embedded in an envelope and only ~ 1 Myr old, where narrow gaps and rings of only a few au wide were detected at $0.04''$ resolution (ALMA Partnership et al. 2015). Similar radial substructures have been seen in several other Class I disks observed at this resolution (Sheehan and Eisner 2018; Segura-Cox et al. 2020), as well as inner cavities with radii > 20 au (Sheehan and Eisner 2017; Sheehan et al. 2020; Alves et al. 2020) and spiral arms (Lee et al. 2020). However, substructure is not seen as commonly and samples are not equivalent in completeness as in the Class II stage (Tobin et al. 2020). Recently, the eDISK ALMA Large Program targeting ~ 20 Class 0 and I disks at $0.04''$ resolution revealed very few disks with substructure, which was interpreted as either rapid planet formation between the Class I and Class II stage, or obscuration of gaps by optical depth effects (Ohashi et al. 2023). The latter is supported by observations of edge-on disks which directly reveal their vertical structure,

showing that even though millimeter-dust is very settled in the Class II stage (Villenave et al. 2020), younger, embedded disks show more flared vertical structures at millimeter wavelengths (Michel et al. 2022; Villenave et al. 2023). Overall the early evolution of substructures in disks remains challenging to constrain, and samples of nearby disks that can be fully spatially resolved are limited to a few dozen. In contrast, the nearby low-mass star forming regions within 200 pc contain ~ 1000 protoplanetary disks for which dust disk properties have been constrained with at least low-resolution imaging (Manara et al. 2022).

During the protoplanetary disk evolution at 1-10 Myr, no clear evolutionary processes have been identified in substructures in disks, as substructures are seen both in the younger 1-3 Myr star forming regions as well as in the older 5-10 Myr regions. Biases and uncertainties in especially the older disk samples make evolutionary effects difficult to assess. Some studies indicate a possible evolutionary link between disks with gaps and disks with cavities, as a growing protoplanet carves a wider gap over time (van der Marel et al. 2018; Cieza et al. 2021), but this cannot be proven with the available small samples and large variety of gap widths.

It is tempting to link the observed substructures in protoplanetary disks to the dusty rings observed in nearby debris disks or ‘exoKuiper belts’, due to their similarity in appearance in dust in the form of rings, gaps, cavities and asymmetries (e.g. Fig. 2 in Marino 2022). However, the dust in debris disks is generated by planetesimal collisions and is no longer coagulating or affected by drag forces in the absence of gas (Hughes et al. 2018), making them fundamentally different from protoplanetary disks. Furthermore, they range in ages anywhere between 10 Myr and 10 Gyr, and their detection rate is heavily limited (and thus biased) by sensitivity, despite many of being much closer than 100 pc. In particular, they are primarily detected around early type stars also after correction for sensitivity (Sibthorpe et al. 2018) and it is challenging to define complete samples as in protoplanetary disk surveys.

When comparing debris disk properties with protoplanetary disks, the dust rings w.r.t. their radius tend to be wider, and a correlation between stellar luminosity and ring radius exists in debris disks, suggesting a link with their formation process, in contrast with dust rings in protoplanetary disks (Marino 2022). One important argument for having a connection is the fact that debris disks require planetesimals to be located at tens of au, and that planetesimals at those radii can grow efficiently in dust traps (Stammler et al. 2019; Pinilla et al. 2020; Miller et al. 2021), whereas pebbles would otherwise drift inwards before growing to boulders and larger (Michel et al. 2021; Najita et al. 2022). However, planetesimal belts need to be dynamically stirred to fragment into detectable debris levels, requiring giant planets inside their dust ring (Wyatt et al. 2015), and a statistical correlation between cold giant planets and debris disks has only been tentatively found so far (Meshkat et al. 2017).

Inner Disk Morphology and Substructures

The inner disk or inner 1 au of protoplanetary disks is particularly interesting in connection with exoplanets, as a large part of the known exoplanet populations (including the rocky planets in our Solar system) reside in this regime. The inner 1 au in protoplanetary disks cannot be spatially resolved with ALMA due to the distances of nearby young disks and the available spatial resolution, as well as the high continuum optical depth in the inner disk. The presence of inner dust disks has been inferred indirectly from near infrared excess in SEDs, in particular in disks with inner cavities (Espaillat et al. 2014). At these distances from the star, dust grains sublimate at ~ 1500 K and the inner edge (sublimation radius) is directly irradiated by the star, resulting in a puffed up wall and resulting strong near infrared emission (Dullemond and Monnier 2010). Optical and infrared see-saw variability can be used to infer more information on azimuthal and/or temporal changes in the inner disk vertical structure due to time-dependent obscuration of the star (Espaillat et al. 2011). Inner dust disks have also been detected at millimeter wavelengths, indicating large grains may be present as well (Francis and van der Marel 2020).

Another way of inferring more information on the structure of the inner dust disk is optical interferometry, e.g. with the VLTI or CHARA arrays at near infrared wavelengths. Inner disk surveys with VLTI instruments such as PIONIER, GRAVITY and recently MATISSE have revealed the geometry of inner dust disks (Menu et al. 2015; Lazareff et al. 2017; Gravity Collaboration et al. 2019; Kluska et al. 2020; Varga et al. 2021; Bohn et al. 2022). Whereas forward imaging is not possible in the same way as with submillimeter interferometry due to the limited uv sampling, radial profiles can be fit to the visibilities and deviations from axisymmetric emission (such as crescents, clumps or protoplanets) can be identified from the closure phase. Such studies are still limited to the brightest systems and samples are thus particularly biased.

Alternatively, infrared molecular line emission originating from the inner region of the disk also provides valuable information about the substructure in the inner disk due to the sublimation of ices frozen out on dust grains that have been transported to the inner part of the disk. The *James Webb Space Telescope (JWST)* is expected to revolutionize this particular field of disk studies, as its sensitivity and spectral resolution exceeds that of *Spitzer*, which means that many additional molecular species will be detectable in larger disk samples. A tentative anti-correlation between infrared H_2O emission as detected with *Spitzer* and disk dust size already hints at the importance of dust transport in setting the chemical composition in the inner part of the disk (Banzatti et al. 2020; Kalyaan et al. 2021). Several first result *JWST* studies indeed show that infrared molecular detections can probe inner disk structures and reveal more about their disk evolution history (Grant et al. 2023; Tabone et al. 2023; Banzatti et al. 2023). A thorough understanding of dust evolution and transport in disks is crucial for a proper interpretation of these new data.

Disk Dust Masses

One of the most fundamental properties of the disk is its total mass, which sets the budget for the planets that can be formed in the disk and that governs the general dynamics in the star-disk system, including gravitational instability. The disk mass has historically been computed as the Minimum Mass Solar Nebula of $\sim 60 M_{\oplus}$ in solids, using the amount of material in the Solar System planets (Hayashi 1981), but can now be derived from protoplanetary disk observations directly, showing a large range in values. Whereas the gas mass is thought to be the dominant contributor at 99% of the disk mass, the dust mass is easier to constrain observationally, and is therefore often used as proxy for the disk mass, assuming a certain gas-to-dust ratio (see end of this section). The dust mass of the disk is generally computed using the integrated millimeter flux, under several assumptions, as follows (Hildebrand 1983).

The integrated flux F_{ν} can be described as the specific intensity I_{ν} integrated over the solid angle $d\Omega$ of the disk:

$$F_{\nu} = \int I_{\nu} d\Omega \quad (12)$$

where I_{ν} is computed from the Planck curve at an assumed temperature T :

$$I_{\nu} = B_{\nu}(T)(1 - e^{-\tau_{\nu}}) \quad (13)$$

where the optical depth τ_{ν} is proportional to the surface density Σ_{dust} and the dust opacity κ_{ν} and scaled with the inclination i :

$$\tau_{\nu} = \frac{\kappa_{\nu} \Sigma_{\text{dust}}}{\cos i} \quad (14)$$

Since the dust mass M_{dust} is the integrated surface density

$$M_{\text{dust}} = \int_0^R \Sigma_{\text{dust}}(r) 2\pi r dr \quad (15)$$

with R the size of the disk, and using

$$d\Omega = \frac{\pi R^2}{d^2} \quad (16)$$

with distance d this can be rewritten as

$$M_{\text{dust}} = \frac{d^2 F_{\nu}}{\kappa_{\nu} B_{\nu}(T)} \quad (17)$$

under the assumption $\tau_{\nu} \ll 1$ so that $1 - e^{-\tau_{\nu}} \approx \tau_{\nu}$, implying that the emission is optically thin and thus represents the entire column. The dust opacity κ_{ν} depends on the grain size distribution and properties (Draine 2006) but is generally assumed as $\kappa_{\nu} = 10 \text{ cm}^2 \text{ g}^{-1}$ at 1000 GHz (Beckwith and Sargent 1991) and scales as $\kappa_{\nu} \sim$

$v^{\beta_{mm}}$ with dust opacity index $\beta_{mm}=1$, hence $\kappa_v=2.3 \text{ cm}^2 \text{ g}^{-1}$ at 230 GHz. For the temperature, $T=20 \text{ K}$ is usually assumed for all disks as a scaling with the stellar luminosity has been shown to make marginal differences (Andrews et al. 2013).

This dust mass calculation is generally used in large disk surveys due to the simple relation with the observed millimeter flux and distance, and can be used to compare (evolutionary) behaviour across samples. Full radiative transfer models that are finetuned to specific disk structures lead to small differences (Andrews and Williams 2007), which can be up to a factor of 2-3 in the presence of large cavities (van der Marel et al. 2018).

Dust Opacity and other Uncertainties

The computed dust mass thus relies heavily on several assumptions: the dust temperature T , the assumed grain properties that set κ_v and the optically thin assumption. They will be discussed one by one.

The dust temperature is generally assumed to be 20 K, under the assumption that the bulk of the dust mass is within that temperature regime. The disk midplane temperature can be approximated by Eqn. 8. One can show that the temperature is $\sim 15\text{-}20 \text{ K}$ outside 20 au for typical stellar luminosities between 0.1 and $1 L_{\odot}$, so if the dust in the disk is typically distributed out to 100 au this is a reasonable assumption for the dust mass calculation. Furthermore, in the Rayleigh-Jeans approximation which is typically valid in the millimeter regime ($h\nu \ll k_B T$) the Planck distribution $B(T)$ can be approximated by:

$$B_v(T(r)) = \frac{2\nu k_B T(r)}{c^2} \quad (18)$$

so the dust mass scales inversely linear with the assumed temperature. It is important to note that if the disk dust size is much smaller than 20 au (which may well be the case for the observed fainter disks, consistent with radial drift), the temperature and thus the dust mass is overestimated by a factor of a few under the assumption of optically thin emission, as illustrated in Figure 7). However, if the dust is optically thick (see below) this effect may be compensated.

The dust opacity is set by the grain size properties, e.g. the maximum grain size a_{\max} , the power q in the size distribution $n(a) \propto a^{-q}$ and the dust composition and porosity (Birnstiel et al. 2018). Several dust opacity tables can be found online, or generated by the user for given properties (see https://github.com/birnstiel/dsharp_opac). The main issue here is that (much) larger grain sizes than the observing wavelength will not significantly contribute to the emission, as the primary contributor at observing wavelength λ_{obs} are grains with size $a = \lambda_{\text{obs}}/2\pi$ (Draine 2006). This means that if a large amount of grains have grown to boulders and planetesimals (see previous section), their total dust mass is larger than the observable dust mass at millimeter wavelengths. The significance of this effect can be as large as two orders of magnitude (Pinilla et al. 2020).

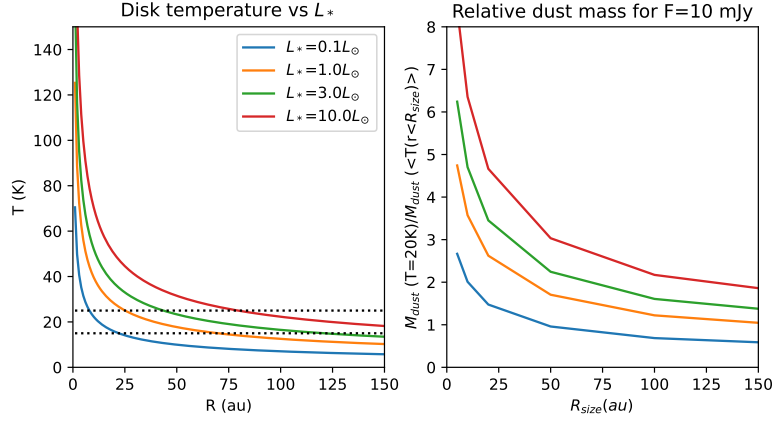


Fig. 7 The effect of the chosen disk temperature on the computed dust mass. The left panel shows the temperature curve from Eqn. 8 for different stellar luminosities. The 15-25 K regime is indicated by dotted lines, showing that the bulk of the outer disk is located around 20 K if the disk is larger than 20 au. The plot on the right shows how much the classical dust mass calculation with $T=20$ K overestimates the actual dust mass assuming the average temperature in the disk for different disk sizes for a flux of 10 mJy at 230 GHz. Especially for disks <20 au in size the classical dust mass is a strong overestimate, which may be compensated by the presence of optically thick emission.

The third uncertainty is the assumption of optically thin emission. If the emission is optically thick, $\tau_\nu > 1$, and Eq. 13 simplifies to $I_\nu = B_\nu$ and the flux no longer scales with Σ_{dust} , but with T . In reality, both density and temperature contribute to the emission, but it implies that the dust mass is underestimated using the observed flux alone. As the optical depth decreases with wavelength, fluxes measured at 3 mm and longer can be more realistically assumed to be optically thin. Multi-wavelength studies including integrated fluxes at longer wavelengths have demonstrated that the amount of optically thick emission is limited in disks and thus does not underestimate the dust mass by more than a factor of a few (Tychoniec et al. 2020; Tazzari et al. 2021a), as most of the optically thick emission is located in the center of the disk when spatially resolved (e.g. Carrasco-González et al. 2019; Macías et al. 2021; Guidi et al. 2022).

Another consequence of optically thick emission is that the dust opacity index β_{mm} , which is generally used to constrain grain growth (see next section) can no longer be derived from the observed spectral index α_{mm} . In the Rayleigh-Jeans (Eqn. 18) and optically thin regime, the flux density from Eqn. 12 scales as

$$F_\nu \propto B_\nu \tau_\nu \propto \nu^2 \kappa_\nu \propto \nu^{2+\beta_{mm}} \quad (19)$$

so the observationally constrained spectral index α_{mm} from $F_\nu \propto \nu^{\alpha_{mm}}$ equals $2+\beta_{mm}$. However, if the emission is optically thick this relation is no longer valid and the grain size can no longer be constrained from the observed spectral index.

Solid Mass Budget

Several disk studies have estimated the solid mass budget available for planet formation during the protoplanetary disk phase using dust continuum observations of large disk samples, using the dust mass derivation above. These dust masses are found to be significantly lower than the solid mass in observed exoplanet cores, suggesting that either planet formation has already finished by the protoplanetary disk phase or that the observed dust masses are severely underestimated (Manara et al. 2018; Tychoniec et al. 2020). A more recent analysis where exoplanet selection and detection biases are taken into account finds that the disk dust masses are in fact comparable to the exoplanet core masses, which would suggest a 100% efficient conversion of dust mass into exoplanet cores, and thus inconsistent with most planet formation models (Mulders et al. 2021b). Although the previous section demonstrates that the dust mass in disks could be underestimated, it is unclear if this is sufficient to explain this discrepancy with exoplanet masses. The alternative explanation is that protoplanetary disks are actually remnants of planet formation, and just reveal the dust that is left. This dust may still grow into planetesimals and form Kuiper belts or asteroid belts. In that case, dust masses of embedded disks rather than protoplanetary disks should be used in planet formation models as initial conditions, which are at least 1 order of magnitude more massive.

Dust Mass Evolution and Trends

Disk dust masses do not only provide initial conditions, but can also be studied in evolutionary context to understand the main processes that dissipate them (Manara et al. 2022). Protoplanetary disk surveys reveal that the general dust mass distribution decreases over time from the Class 0 to the Class III and debris disk stage over several orders of magnitude (Cieza et al. 2019; Williams et al. 2019; Michel et al. 2021, and Figure 9). As the dust mass is correlated with the dust disk size (Tripathi et al. 2017), it is not surprising that the observed disk dust size decreases with age as well during the Class II phase (Hendler et al. 2020; Tazzari et al. 2021a). Some correlation exists between the dust mass and the disk accretion rate (Manara et al. 2016), but the scatter in this correlation is large, casting doubts on their physical relation (Manara et al. 2020).

Furthermore, the dust mass correlates with the stellar mass, albeit with large scatter, although the slope of this correlation steepens over time, indicating that the dust mass decreases more rapidly for lower mass stars (Ansdell et al. 2017, and Figure 8). When disks with dust rings and gaps are considered separately, their correlation with stellar mass is much flatter than the majority of disks (Pinilla et al. 2018). The main correlation implies that higher mass stars generally have higher mass disks, but considering the scatter in this relation, it should be noted that a small fraction of disks around low-mass stars (M-dwarfs) do have higher mass disks,

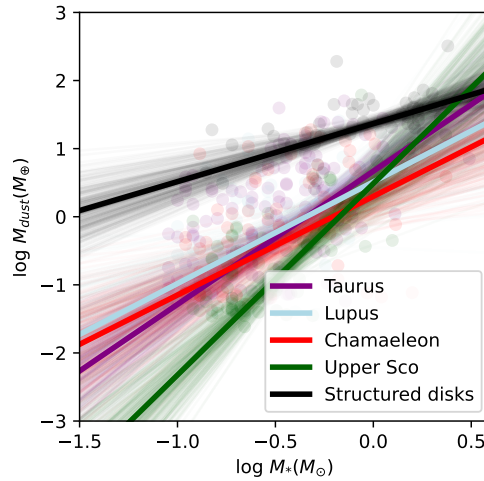


Fig. 8 Observed correlation between dust mass and stellar mass, using data from ALMA surveys of nearby star forming regions between 1 and 10 Myr. Note that Ophiuchus disks (Cieza et al. 2019) are not included as the known stellar masses are incomplete. The different regions are color-coded according to the legend. Transparent circles represent the data points, the solid lines represent the best-fit linear correlations using the `linmix` python package to include upper limits, with the grey lines representing the spread in the fit. The structured disks containing dust traps (disks with cavities and gaps) are grouped separately from the regions. All data points (van der Marel and Mulders 2021) are corrected for their Gaia DR2 distance. The plot shows that the correlation between dust mass and stellar mass steepens with time (Ansdell et al. 2017) but structured disks with dust traps follow a flatter relation (Pinilla et al. 2020).

perhaps even massive enough to form giant planets or to contain remnants of giant planet formation (Curone et al. 2022).

Whereas there is still active debate on the general mechanism of gas dissipation in the disk (viscously driven or driven by a magnetohydrodynamical wind, or both, see Manara et al. (2022)), in recent years it has been proposed that the dust evolution is decoupled from the gas disk evolution (Sellek et al. 2020). Disk models including radial drift (see first section) can reproduce the observed trends in dust mass for the majority of disks, including the stellar mass dependence (Pinilla et al. 2020; Zormpas et al. 2022; Appalgren et al. 2023). This implies that the observed dust mass is not representative for the disk mass, and gas-to-dust ratios may be much larger than the ISM ratio of 100 for such disks (see later discussion), if the radial drift is well on its way by the time the dust mass is observed. On the other hand, the amount of millimeter-dust in pressure bumps does not decrease by radial drift and the dust mass would remain high, but this would be only a small fraction of the full disk population considering the general trends. This would explain the massive outliers with dust traps seen in some older star forming regions (Ansdell et al. 2020). A scenario of separate evolutionary pathways for disks with and without dust traps

has been proposed (van der Marel and Mulders 2021, and Figure 9), but remains to be confirmed by more uniformly observed disk data.

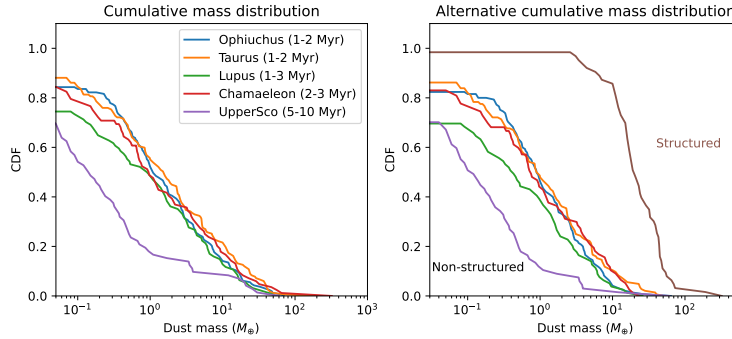


Fig. 9 Cumulative mass distribution function of dust masses of Class II disks, using data from ALMA surveys of nearby star forming regions between 1 and 10 Myr, computed with the `lifelines` python package to take into account upper limits. The left plot shows the result of the full disk populations in each region, similar to Cieza et al. (2019), the right plot considers the disks with structure (disks with cavities and gaps) and without structure separately, following van der Marel and Mulders (2021). These plots demonstrate that the dust mass of the majority of disks decreases with age as the result of radial drift, whereas the dust mass of structured disks stays on the high end of the distribution.

Gas-to-Dust Ratio

The observed dust mass is often used to compute a gas mass by multiplying with the ISM gas-to-dust ratio of 100, to infer the total disk mass. Alternative methods using molecular line observations such as HD and CO isotopologues to infer the gas-to-dust ratio suggest that the ratio may be at least an order of magnitude lower, either due to increased gas dissipation, inaccuracies in the conversion from CO to H₂, or both. A full discussion of these uncertainties is beyond the scope of this chapter, but a review on the relevant aspects and consequences for disk gas masses has been written by Miotello et al. (2022). Furthermore, the uncertainties in the dust mass calculation and the dust evolution processes cast further doubt on the validity of using a universal gas-to-dust ratio to compute disk gas masses.

Dust Growth

Spectral Index and Grain Sizes

Submillimetre and microwave emission from the diffuse interstellar dust have shown that the typical values for the dust opacity index β_{mm} (see previous section) in this media is 1.7-2.0 (Finkbeiner et al. 1999). Understanding how the opacity index varies in protoplanetary disks has been a driver for multi-wavelength observations in the last decade. If the dust in protoplanetary disks has a similar size distribution as in the interstellar medium, the opacity index should be similar. However, it has been found that the opacity index is (much) lower than 1.7, suggesting that dust grains are growing in disks (Draine 2006).

The usual method to obtain the opacity index of protoplanetary disks is by assuming that the (sub-) millimeter emission is optically thin and in the Rayleigh-Jeans limit is directly proportional to the observed millimeter spectral index α_{mm} , such that $\beta_{\text{mm}} = \alpha_{\text{mm}} - 2$ (Eq. 19). By measuring the total millimeter flux of protoplanetary disks, the spatially integrated β_{mm} is less than 1.7 for disks in different star forming regions, for a large range of disk luminosities and types of stars. This indicates that large millimeter-sized particles are present in protoplanetary disks with different properties (e.g., Beckwith and Sargent 1991; Testi et al. 2001; Ricci et al. 2010; Guilloteau et al. 2011; Tazzari et al. 2021b). High angular resolution observations that are sufficient to resolve spatial variations of the spectral index, have shown that it increases in the outer disk (as expected from dust evolution models, where the larger grains are located in the inner parts (e.g., Pérez et al. 2015; Tazzari et al. 2021b)), and the spectral index seems to decrease inside disk substructures, suggesting that these regions are preferential for grain growth (e.g., Casassus et al. 2015; van der Marel et al. 2015; Carrasco-González et al. 2019; Guidi et al. 2022). Current interpretations of the spectral index are limited because the emission in submillimeter images is not fully optically thin and because the effect of dust self-scattering is neglected.

(Sub-)millimeter-wave Polarization

Polarization at sub-millimeter wavelengths has been detected in young disks (Class 0-I) as well as in more evolved disks (Class II) (Rao et al. 2014; Cox et al. 2015; Kataoka et al. 2017). This polarization is usually interpreted by grain alignment perpendicular to the magnetic field, radiation flux, or by dust self-scattering (Andersson et al. 2015, for a review). The polarization patterns by dust self-scattering can also provide insights about the grain size in protoplanetary disks.

This can be understood as follows: when dust grains in protoplanetary disks emit thermal radiation, this emission can be scattered by other dust grains, hence called 'self-scattering'. Dust grains that are comparable to or larger than the observing

wavelength, $a > \lambda/2\pi$, are expected to have a large albedo, so that their scattering efficiency is high enough to produce scattered emission. An efficient polarization is reached for $a \sim \lambda/2\pi$ because for grains much larger than the observing wavelength the scattering is strongly forward peaked, and no polarization is expected. Polarization observations at sub-millimeter wavelengths of a handful of disks suggest that the maximum grain size is around 100-150 μm (e.g., Kataoka et al. 2016, 2017), but when multi-wavelength polarization maps are analysed, it is difficult to find a single mechanism that could explain the detected polarization in protoplanetary disks (Tang et al. 2023) and provide a maximum grain size. Additionally, the interpretation of millimetre polarization observations can become more complex in the presence of pressure bumps (Pohl et al. 2016).

Exoplanet Populations and Trends w.r.t. Disks

Exoplanets are generally grouped by their mass and location in different populations, each with their own trends on their occurrence rate w.r.t. stellar mass, metallicity and orbital radius, for example super-Earths and sub-Neptunes, gas giants, wide-orbit (super-)Jupiter planets and rocky planets. As the exoplanet population is so diverse, the disk population should reflect this diversity as well if planet formation dominates the disk processes and their resulting appearance, at least after corrections for detection and selection biases (Drazkowska et al. 2022).

Gapped Disks and Giant Planets

One of the most obvious connections are the disks with large inner gaps w.r.t. wide orbit giant planets from high contrast imaging, as deep gaps require massive protoplanets or at least massive planet cores at large orbital radii at tens of au to carve them. Initial comparisons between the fraction of transition disks with inner cavities >20 au and the fraction of wide orbit giant planets at 10-100 au indicated strong discrepancies as the transition disk fraction of $11 \pm 3\%$ is significantly higher than the limits on wide orbit super-Jupiter occurrence of $<4\%$ for FGK stars (e.g. van der Marel et al. 2018). Also for disks with narrow gaps at tens of au for which a sub-Jupiter mass is sufficient (Lambrechts et al. 2019), the giant exoplanet population appears to be inconsistent as the occurrence of giant exoplanets peaks at 2-6 au and drops to a few % at larger radii (e.g. Fulton et al. 2021). The obvious solution to this problem is inward migration of these planets after they have created the gaps observed in disks to the location where they are observed today in the exoplanet population (Lodato et al. 2019). Even then, high-resolution disk observations appear to suggest that gapped disks are much more numerous than unstructured disks, inconsistent with the typical occurrences of giant exoplanets of $\sim 20\text{-}25\%$ (Fernandes et al. 2019; Fulton et al. 2021).

The observational bias in protoplanetary disks studies (see Figure 6) may play an important role here though, as discussed previously, as primarily brighter disks around higher mass stars have been imaged at high angular resolution (Bae et al. 2022a). For example, the DSHARP survey discovered substructure in all disks imaged at $0.04''$ resolution (Andrews et al. 2018), but pre-selected disks that had been previously spatially resolved by ALMA and were thus by definition extended and bright. The unbiased Taurus disk survey by Long et al. (2019) suggested that around half of the disks around single stars contain substructure, but this survey only considered stars with spectral type $<M2$ (stellar masses $>0.5 M_{\odot}$).

Estimates of the fraction of disks that contain large-scale gaps in a very large disk survey (van der Marel and Mulders 2021) range from 10-20% when considering stellar masses from 0.1 to $3 M_{\odot}$, much closer to the giant exoplanet occurrence rate, with the caution that not all disks have been sufficiently spatially resolved to rule out gaps. More specifically, they revealed a stellar mass dependence of the gapped disks for stars between 0.1 and $2.5 M_{\odot}$, ranging from a few % for M-dwarfs up to more than 60% for stars $>1.5 M_{\odot}$, very similar to the stellar mass dependence of giant exoplanets (Figure 10). A stellar mass dependence was also found for a sample of transition disks with large inner cavities (van der Marel 2023) and a Herbig survey shows a fraction of more than 50% of gapped disks, much higher than that of T Tauri stars (Stapper et al. 2021).

The main shortcoming of these surveys is the lack of knowledge on substructures on smaller scales, in particular in the fainter disks. Only uniform high-resolution observations of full disk samples can fully confirm the validity of the stellar mass dependence. New imaging techniques have revealed subtle substructures in the inner part of some smooth, compact disks (Jennings et al. 2022). Also, at least one bright protoplanetary disk showed no evidence for substructure at $0.05''$ despite being radially extended (Ribas et al. 2023). Fully complete surveys at high angular resolution should provide better clues on the disk demographics and the significance of these trends.

Compact Disks and Super-Earths

A stellar mass dependence of gapped disks implies an opposite trend for drift-dominated disks: disks around low-mass stars are more likely to contain no large-scale dust traps and are thus more often very compact (<20 au) in size (Figure 10). Furthermore, the drift efficiency has been shown to be more efficient around low-mass stars, as discussed in the first section of this chapter. Such disks often remain unresolved in low-resolution ALMA disk surveys, with upper limits on the dust size radius of <15 au up to at most ~ 40 au, which makes it challenging to confirm their nature as smooth, compact disks without substructure. Only a handful of compact disks has been radially resolved at a few au resolution with sizes of 3-10 au radius (Facchini et al. 2019; Kurtovic et al. 2021; van der Marel et al. 2022). Their existence may be most evident from inner disk molecular content: if pebbles drift inward

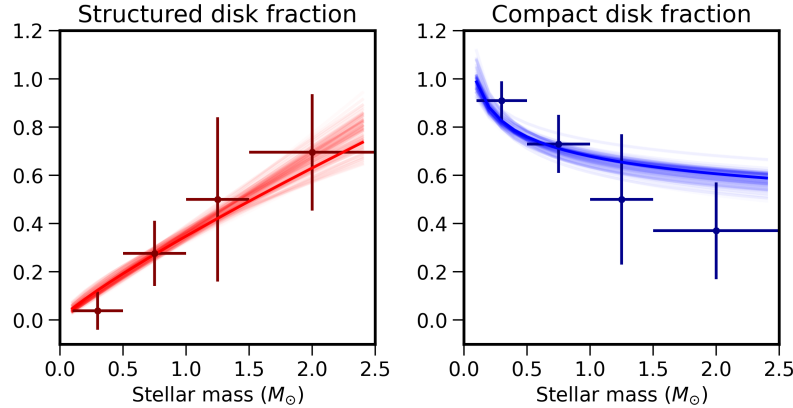


Fig. 10 The stellar mass dependence of disks with large-scale substructure and that of compact disks, based on the data from van der Marel and Mulders (2021). These plots follow their Figure 7 for the combined structured disks (including transition disks, gapped disks and extended disks >40 au) and the compact disks (defined as disks <40 au in radius without observed substructure), not yet computed there. The plot shows a comparison between the computed disk fractions at pre-defined stellar mass bins (points with error bars) and the disk fraction estimated from a power-law fit (solid lines). The transparent lines indicate the spread in MCMC samples from the fit. The disk sample contains more than 500 disks from nearby star forming regions observed at a range of angular resolutions. The plot demonstrates that gapped disks are more common around high-mass stars whereas compact disks are most common around M-dwarfs.

the H_2O snowline which is typically inside 1 au, their icy layers evaporate and increase the gaseous H_2O content, which can be measured with infrared facilities like *Spitzer* and *JWST* (Kalyaan et al. 2021, 2023). An increased H_2O content has indeed been measured for compact dust disks (Banzatti et al. 2020, 2023), confirming their pebble drift nature.

The population of drift-dominated disks could be natural sites for close-in super-Earth formation, due to the increased pebble rates in the inner part of the disk as a result of the radial drift (Lambrechts et al. 2019; Mulders et al. 2021a). Close-in super-Earths (‘Kepler planets’) are particularly common in M-dwarfs (Mulders 2018), following thus the trend seen in disks. Such planets can only be formed efficiently when the drift is not halted by the presence of a cold giant planet further out. This may contradict with the tentative correlation between close-in super-Earths and cold giants (Zhu and Wu 2018; Bryan et al. 2019; Fulton et al. 2021), but this trend remains to be confirmed for low-mass stars.

Stellar Metallicity

A second important trend in exoplanet populations is the correlation between the occurrence rate of giant planets with metallicity (Fischer and Valenti 2005), which

disappears for super-Earths and sub-Neptunes (Buchhave et al. 2014; Kutra et al. 2021). Whether such a trend with metallicity can be related to protoplanetary disks remains a topic of debate (Drazkowska et al. 2022).

Elemental abundances of the hosting stars are expected to be sensitive to different disk evolution processes, in particular efficient radial drift. Dust drift can enrich the stellar abundance of refractory elements at early times (Hühn and Bitsch 2023). However, if trapping of dust particles occurs blocking the inward drifting particles (for example by a giant planet), the stellar refractory elements should decrease. The current correlation between more metal rich stars likely hosting more massive planets indicates that either the effect of the formation of the giant planet planets in their parental disk on the stellar photosphere was erased with the stellar evolution, possibly by the mixing of their convective envelope; or the observed correlation with the present-time values was stronger at earlier times.

Stars more massive than the Sun, have a radiative envelope rather than a convective envelope, which leads to slower mixing. Hence, for these stars ($\gtrsim 1-1.4 M_{\odot}$), the stellar photospheres can be dominated by the recent accretion of material and thus these stars are good candidates to test enrichment of refractory elements by dust drift. Kama et al. (2015) demonstrated that there is a correlation between the presence of large disk cavities (that are likely caused by dust trapping) and the depletion of refractory elements of a set of Herbig Ae/Be stars. This conclusion was confirmed in Kama et al. (2019) by measuring the refractory sulfur in the photospheres of a sample of young stars with a mass of $> 1.4 M_{\odot}$, finding that Sulfur abundance is lower when trapping happened, presumably by a giant planet. For these stars, the inner disk abundance should be reflected in the stellar photosphere, which is supported by the results from Banzatti et al. (2018) who finds that the NIR excess of protoplanetary disks strongly relates to the Fe/H ratios in stellar atmospheres.

The expected correlations between stellar metallicity and the type of planets forming around should depend then on the type of star (stars with mass lower than $\sim 1 M_{\odot}$ have a convective envelope and hence faster mixing), but also a dependency with the drift efficiency is expected, which is connected with the open questions of when giant planets form, the disk viscosity, and the micro-physical properties of dust particles, such as their fragmentation velocity.

Outlook

The revolution of observational work in protoplanetary disk studies has resulted in numerous new insights in disk processes and planet formation. State-of-the-art models can now be compared much more directly to observations, revealing clues to the processes happening in these disks. As demonstrated in this chapter, the field of protoplanetary disks still suffers from several observational biases, and key for future development will be more uniform studies of larger samples across the IMF for proper comparisons with exoplanet properties. Higher sensitivity, as provided by ALMA in the Wideband Sensitivity Upgrade in the 2030s, will allow more rapid

imaging of even the faintest disks in the nearby Universe. The *James Webb Space Telescope* has only just started to deliver observations tracing the chemical composition in the warm regions of the disks, which may be highly important in constraining the dust structure in the terrestrial regime of the disk. Ground-based optical/infrared facilities are expecting major upgrades increasing sensitivity and improvements in the adaptive optics system and the Extremely Large Telescope (ELT) will provide another jump in sensitivity and resolution in infrared imaging of disks. At longer wavelengths, the next generation Very Large Array (ngVLA) and the Square Kilometer Array (SKA) are expected to trace the distribution of larger, centimeter-sized pebbles to shed further light on the dust growth and planet formation processes in protoplanetary disks.

Cross-References

- Imaging with Adaptive Optics and Coronagraphs for Exoplanet Research
- Planet Populations as a Function of Stellar Properties
- A Brief Overview of Planet Formation
- Chemistry During the Gas-Rich Stage of Planet Formation
- Instabilities and Flow Structures in Protoplanetary Disks: Setting the Stage for Planetesimal Formation
- Planetary Migration in Protoplanetary Disks
- Formation of Giant Planets
- Formation of Super-Earths
- Debris Disks: Probing Planet Formation
- Circumstellar Discs: What Will Be Next?

Acknowledgements The authors thank Takayuki Muto, Mariana Sanchez and Sid Gandhi for providing useful comments on this manuscript.

References

- Alexander RD, Clarke CJ Pringle JE (2006) Photoevaporation of protoplanetary discs - II. Evolutionary models and observable properties. *MNRAS*369(1):229–239
- ALMA Partnership A, Brogan CL, Pérez LM et al. (2015) The 2014 ALMA Long Baseline Campaign: First Results from High Angular Resolution Observations toward the HL Tau Region. *ApJ*808:L3
- Alves FO, Cleeves LI, Girart JM et al. (2020) A Case of Simultaneous Star and Planet Formation. *ApJ*904(1):L6
- Andersson BG, Lazarian A Vaillancourt JE (2015) Interstellar Dust Grain Alignment. *ARA&A*53:501–539
- Andrews SM (2020) Observations of Protoplanetary Disk Structures. *ARA&A*58:483–528
- Andrews SM Williams JP (2007) High-Resolution Submillimeter Constraints on Circumstellar Disk Structure. *ApJ*659:705–728

- Andrews SM, Wilner DJ, Espaillat C et al. (2011) Resolved Images of Large Cavities in Protoplanetary Transition Disks. *ApJ*732:42
- Andrews SM, Rosenfeld KA, Kraus AL Wilner DJ (2013) The Mass Dependence between Protoplanetary Disks and their Stellar Hosts. *ApJ*771:129
- Andrews SM, Wilner DJ, Zhu Z et al. (2016) Ringed Substructure and a Gap at 1 au in the Nearest Protoplanetary Disk. *ApJ*820:L40
- Andrews SM, Huang J, Pérez LM et al. (2018) The Disk Substructures at High Angular Resolution Project (DSHARP). I. Motivation, Sample, Calibration, and Overview. *ApJ*869:L41
- Ansdell M, Williams JP, van der Marel N et al. (2016) ALMA Survey of Lupus Protoplanetary Disks. I. Dust and Gas Masses. *ApJ*828:46
- Ansdell M, Williams JP, Manara CF et al. (2017) An ALMA Survey of Protoplanetary Disks in the σ Orionis Cluster. *AJ*153:240
- Ansdell M, Gaidos E, Hedges C et al. (2020) Are inner disc misalignments common? ALMA reveals an isotropic outer disc inclination distribution for young dipper stars. *MNRAS*492(1):572–588
- Appelgren J, Lambrechts M van der Marel N (2023) Disc population synthesis: Decrease in the solid mass reservoir through pebble drift. *A&A*673:A139
- Artymowicz P Lubow SH (1996) Mass Flow through Gaps in Circumbinary Disks. *ApJ*467:L77
- Asensio-Torres R, Henning T, Cantalloube F et al. (2021) Perturbers: SPHERE detection limits to planetary-mass companions in protoplanetary disks. *A&A*652:A101
- Ataiee S, Pinilla P, Zsom A et al. (2013) Asymmetric transition disks: Vorticity or eccentricity? *A&A*553:L3
- Ataiee S, Baruteau C, Alibert Y Benz W (2018) How much does turbulence change the pebble isolation mass for planet formation? *A&A*615:A110
- Bae J, Pinilla P Birnstiel T (2018) Diverse Protoplanetary Disk Morphology Produced by a Jupiter-mass Planet. *ApJ*864(2):L26
- Bae J, Isella A, Martin R et al. (2022a) Structured Distributions of Gas and Solids in Protoplanetary Disks. *Protostars and Planets VII*
- Bae J, Teague R, Andrews SM et al. (2022b) Molecules with ALMA at Planet-forming Scales (MAPS): A Circumplanetary Disk Candidate in Molecular-line Emission in the AS 209 Disk. *ApJ*934(2):L20
- Bai XN Stone JM (2013) Wind-driven Accretion in Protoplanetary Disks. I. Suppression of the Magnetorotational Instability and Launching of the Magnetocentrifugal Wind. *ApJ*769(1):76
- Banzatti A, Pinilla P, Ricci L et al. (2015) Direct Imaging of the Water Snow Line at the Time of Planet Formation using Two ALMA Continuum Bands. *ApJ*815(1):L15
- Banzatti A, Garufi A, Kama M et al. (2018) Observing the linked depletion of dust and CO gas at 0.1-10 au in disks of intermediate-mass stars. *A&A*609:L2
- Banzatti A, Pascucci I, Bosman AD et al. (2020) Hints for Icy Pebble Migration Feeding an Oxygen-rich Chemistry in the Inner Planet-forming Region of Disks. *ApJ*903(2):124
- Banzatti A, Pontoppidan KM, Carr J et al. (2023) JWST reveals excess cool water near the snowline in compact disks, consistent with pebble drift. *arXiv e-prints arXiv:2307.03846*
- Barge P Sommeria J (1995) Did planet formation begin inside persistent gaseous vortices? *A&A*295:L1–L4
- Baruteau C Zhu Z (2016) Gas and dust hydrodynamical simulations of massive lopsided transition discs - II. Dust concentration. *MNRAS*458:3927–3941
- Beckwith SVW Sargent AI (1991) Particle Emissivity in Circumstellar Disks. *ApJ*381:250
- Benisty M, Bae J, Facchini S et al. (2021) A Circumplanetary Disk around PDS70c. *ApJ*916(1):L2
- Benisty M, Dominik C, Follette K et al. (2022) Optical and Near-infrared View of Planet-forming Disks and Protoplanets. *arXiv e-prints arXiv:2203.09991*
- Birnstiel T, Dullemond CP Brauer F (2010) Gas- and dust evolution in protoplanetary disks. *A&A*513:A79
- Birnstiel T, Dullemond CP Pinilla P (2013) Lopsided dust rings in transition disks. *A&A*550:L8
- Birnstiel T, Fang M Johansen A (2016) Dust Evolution and the Formation of Planetesimals. *Space Sci Rev*205(1-4):41–75

- Birnstiel T, Dullemond CP, Zhu Z et al. (2018) The Disk Substructures at High Angular Resolution Project (DSHARP). V. Interpreting ALMA Maps of Protoplanetary Disks in Terms of a Dust Model. *ApJ*869(2):L45
- Blum J Wurm G (2000) Experiments on Sticking, Restructuring, and Fragmentation of Preplanetary Dust Aggregates. *Icarus*143(1):138–146
- Bohn AJ, Benisty M, Perraut K et al. (2022) Probing inner and outer disk misalignments in transition disks. Constraints from VLTI/GRAVITY and ALMA observations. *A&A*658:A183
- Booth AS, Walsh C, Terwisscha van Scheltinga J et al. (2021) An inherited complex organic molecule reservoir in a warm planet-hosting disk. *Nature Astronomy* 5:684–690
- Booth AS, Ilee JD, Walsh C et al. (2023) Sulphur monoxide emission tracing an embedded planet in the HD 100546 protoplanetary disk. *A&A*669:A53
- Brauer F, Dullemond CP Henning T (2008) Coagulation, fragmentation and radial motion of solid particles in protoplanetary disks. *A&A*480(3):859–877
- Brown JM, Blake GA, Qi C, Dullemond CP Wilner DJ (2008) LkH α 330: Evidence for Dust Clearing through Resolved Submillimeter Imaging. *ApJ*675:L109–L112
- Brown JM, Blake GA, Qi C et al. (2009) Evidence for Dust Clearing Through Resolved Submillimeter Imaging. *ApJ*704:496–502
- Bryan ML, Knutson HA, Lee EJ et al. (2019) An Excess of Jupiter Analogs in Super-Earth Systems. *AJ*157(2):52
- Buchhave LA, Bizzarro M, Latham DW et al. (2014) Three regimes of extrasolar planet radius inferred from host star metallicities. *Nature*509(7502):593–595
- Carrasco-González C, Sierra A, Flock M et al. (2019) The Radial Distribution of Dust Particles in the HL Tau Disk from ALMA and VLA Observations. *ApJ*883(1):71
- Casassus S, Wright CM, Marino S et al. (2015) A Compact Concentration of Large Grains in the HD 142527 Protoplanetary Dust Trap. *ApJ*812:126
- Cazzoletti P, van Dishoeck EF, Pinilla P et al. (2018) Evidence for a massive dust-trapping vortex connected to spirals. Multi-wavelength analysis of the HD 135344B protoplanetary disk. *A&A*619:A161
- Christiaens V, Casassus S, Perez S, van der Plas G Ménard F (2014) Spiral Arms in the Disk of HD 142527 from CO Emission Lines with ALMA. *ApJ*785:L12
- Cieza LA, Ruíz-Rodríguez D, Hales A et al. (2019) The Ophiuchus DIsc Survey Employing ALMA (ODISEA) - I: project description and continuum images at 28 au resolution. *MNRAS*482(1):698–714
- Cieza LA, González-Ruilova C, Hales AS et al. (2021) The Ophiuchus DIsc Survey Employing ALMA (ODISEA) - III. The evolution of substructures in massive discs at 3-5 au resolution. *MNRAS*501(2):2934–2953
- Cox EG, Harris RJ, Looney LW et al. (2015) High-resolution 8 mm and 1 cm Polarization of IRAS 4A from the VLA Nascent Disk and Multiplicity (VANDAM) Survey. *ApJ*814:L28
- Curone P, Izquierdo AF, Testi L et al. (2022) A giant planet shaping the disk around the very low-mass star CIDA 1. *A&A*665:A25
- Currie T, Lawson K, Schneider G et al. (2022) Images of embedded Jovian planet formation at a wide separation around AB Aurigae. *Nature Astronomy* 6:751–759
- de Juan Ovelar M, Pinilla P, Min M, Dominik C Birnstiel T (2016) Constraining turbulence mixing strength in transitional discs with planets using SPHERE and ALMA. *MNRAS*459(1):L85–L89
- Delage TN, Okuzumi S, Flock M, Pinilla P Dzyurkevich N (2022) Steady-state accretion in magnetized protoplanetary disks. *A&A*658:A97
- Delage TN, Gárate M, Okuzumi S et al. (2023) The impact of dust evolution on the dead zone outer edge in magnetized protoplanetary disks. *A&A*674:A190
- Dong R, Zhu Z, Rafikov RR Stone JM (2015a) Observational Signatures of Planets in Protoplanetary Disks: Spiral Arms Observed in Scattered Light Imaging Can Be Induced by Planets. *ApJ*809:L5
- Dong R, Zhu Z Whitney B (2015b) Observational Signatures of Planets in Protoplanetary Disks I. Gaps Opened by Single and Multiple Young Planets in Disks. *ApJ*809:93

- Dong R, van der Marel N, Hashimoto J et al. (2017) The Sizes and Depletions of the Dust and Gas Cavities in the Transitional Disk J160421.7-213028. *ApJ*836:201
- Dong R, Liu SY Fung J (2019) Observational Signatures of Planets in Protoplanetary Disks: Planet-induced Line Broadening in Gaps. *ApJ*870(2):72
- Dotter A, Chaboyer B, Jevremović D et al. (2008) The Dartmouth Stellar Evolution Database. *ApJS*178(1):89–101
- Draine BT (2006) On the Submillimeter Opacity of Protoplanetary Disks. *ApJ*636(2):1114–1120
- Drazkowska J, Bitsch B, Lambrechts M et al. (2022) Planet Formation Theory in the Era of ALMA and Kepler: from Pebbles to Exoplanets. *arXiv e-prints arXiv:2203.09759*
- Dullemond CP Monnier JD (2010) The Inner Regions of Protoplanetary Disks. *ARA&A*48:205–239
- Dullemond CP, Birnstiel T, Huang J et al. (2018) The Disk Substructures at High Angular Resolution Project (DSHARP). VI. Dust Trapping in Thin-ringed Protoplanetary Disks. *ApJ*869(2):L46
- Españolat C, Furlan E, D’Alessio P et al. (2011) A Spitzer IRS Study of Infrared Variability in Transitional and Pre-transitional Disks Around T Tauri Stars. *ApJ*728:49
- Españolat C, Muzerolle J, Najita J et al. (2014) An Observational Perspective of Transitional Disks. *Protostars and Planets VI* pp 497–520
- Facchini S, Pinilla P, van Dishoeck EF de Juan Ovelar M (2018) Inferring giant planets from ALMA millimeter continuum and line observations in (transition) disks. *A&A*612:A104
- Facchini S, van Dishoeck EF, Manara CF et al. (2019) High gas-to-dust size ratio indicating efficient radial drift in the mm-faint CX Tauri disk. *A&A*626:L2
- Fernandes RB, Mulders GD, Pascucci I, Mordasini C Emsenhuber A (2019) Hints for a Turnover at the Snow Line in the Giant Planet Occurrence Rate. *ApJ*874(1):81
- Finkbeiner DP, Davis M Schlegel DJ (1999) Extrapolation of Galactic Dust Emission at 100 Microns to Cosmic Microwave Background Radiation Frequencies Using FIRAS. *ApJ*524(2):867–886
- Fischer DA Valenti J (2005) The Planet-Metallicity Correlation. *ApJ*622(2):1102–1117
- Flaherty K, Hughes AM, Simon JB et al. (2020) Measuring Turbulent Motion in Planet-forming Disks with ALMA: A Detection around DM Tau and Nondetections around MWC 480 and V4046 Sgr. *ApJ*895(2):109
- Flaherty KM, Hughes AM, Rosenfeld KA et al. (2015) Weak Turbulence in the HD 163296 Protoplanetary Disk Revealed by ALMA CO Observations. *ApJ*813(2):99
- Flock M, Ruge JP, Dzyurkevich N et al. (2015) Gaps, rings, and non-axisymmetric structures in protoplanetary disks. From simulations to ALMA observations. *A&A*574:A68
- Francis L van der Marel N (2020) Dust-depleted Inner Disks in a Large Sample of Transition Disks through Long-baseline ALMA Observations. *ApJ*892(2):111
- Fulton BJ, Rosenthal LJ, Hirsch LA et al. (2021) California Legacy Survey. II. Occurrence of Giant Planets beyond the Ice Line. *ApJS*255(1):14
- Fung J Chiang E (2016) Gap Opening in 3D: Single-planet Gaps. *ApJ*832(2):105
- Gárate M, Birnstiel T, Drazkowska J Stammer SM (2020) Gas accretion damped by dust back-reaction at the snow line. *A&A*635:A149
- Gárate M, Delage TN, Stadler J et al. (2021) Large gaps and high accretion rates in photoevaporative transition disks with a dead zone. *A&A*655:A18
- Gonzalez JF, Pinte C, Maddison ST, Ménard F Fouchet L (2012) Planet gaps in the dust layer of 3D protoplanetary disks. II. Observability with ALMA. *A&A*547:A58
- Grant SL, van Dishoeck EF, Tabone B et al. (2023) MINDS. The Detection of $^{13}\text{CO}_2$ with JWST-MIRI Indicates Abundant CO_2 in a Protoplanetary Disk. *ApJ*947(1):L6
- Gravity Collaboration, Perraut K, Labadie L et al. (2019) The GRAVITY Young Stellar Object survey. I. Probing the disks of Herbig Ae/Be stars in terrestrial orbits. *A&A*632:A53
- Guidi G, Isella A, Testi L et al. (2022) Distribution of solids in the rings of the HD 163296 disk: a multiwavelength study. *A&A*664:A137

- Guilloteau S, Dutrey A, Piétu V, Boehler Y (2011) A dual-frequency sub-arcsecond study of protoplanetary disks at mm wavelengths: first evidence for radial variations of the dust properties. *A&A*529:A105
- Gundlach B, Schmidt KP, Kreuzig C et al. (2018) The tensile strength of ice and dust aggregates and its dependence on particle properties. *MNRAS*479(1):1273–1277
- Haffert SY, Bohn AJ, de Boer J et al. (2019) Two accreting protoplanets around the young star PDS 70. *Nature Astronomy* 3:749–754
- Hammond I, Christiaens V, Price DJ et al. (2023) Confirmation and Keplerian motion of the gap-carving protoplanet HD 169142 b. *MNRAS*522(1):L51–L55
- Hayashi C (1981) Structure of the Solar Nebula, Growth and Decay of Magnetic Fields and Effects of Magnetic and Turbulent Viscosities on the Nebula. *Progress of Theoretical Physics Supplement* 70:35–53
- Hendler N, Pascucci I, Pinilla P et al. (2020) The Evolution of Dust Disk Sizes from a Homogeneous Analysis of 1-10 Myr old Stars. *ApJ*895(2):126
- Hernández J, Hartmann L, Megeath T et al. (2007) A Spitzer Space Telescope Study of Disks in the Young σ Orionis Cluster. *ApJ*662:1067–1081
- Hildebrand RH (1983) The Determination of Cloud Masses and Dust Characteristics from Submillimetre Thermal Emission. *QJRAS*24:267
- Huang J, Andrews SM, Dullemond CP et al. (2018) The Disk Substructures at High Angular Resolution Project (DSHARP). II. Characteristics of Annular Substructures. *ApJ*869(2):L42
- Hughes AM, Duchêne G, Matthews BC (2018) Debris Disks: Structure, Composition, and Variability. *ARA&A*56:541–591
- Hühn LA, Bitsch B (2023) How does accretion of planet-forming disks influence stellar abundances? *arXiv e-prints* arXiv:2306.16461
- Isella A, Guidi G, Testi L et al. (2016) Ringed Structures of the HD 163296 Protoplanetary Disk Revealed by ALMA. *Physical Review Letters* 117(25):251101
- Jennings J, Tazzari M, Clarke CJ, Booth RA, Rosotti GP (2022) Superresolution trends in the ALMA Taurus survey: structured inner discs and compact discs. *MNRAS*514(4):6053–6073
- Jiang H, Zhu W, Ormel CW (2022) No Significant Correlation between Line-emission and Continuum Substructures in the Molecules with ALMA at Planet-forming Scales Program. *ApJ*924(2):L31
- Johansen A, Oishi JS, Mac Low MM et al. (2007) Rapid planetesimal formation in turbulent circumstellar disks. *Nature*448:1022–1025
- Juhász A, Benisty M, Pohl A et al. (2015) Spiral arms in scattered light images of protoplanetary discs: are they the signposts of planets? *MNRAS*451:1147–1157
- Kalyaan A, Pinilla P, Krijt S, Mulders GD, Banzatti A (2021) Linking Outer Disk Pebble Dynamics and Gaps to Inner Disk Water Enrichment. *ApJ*921(1):84
- Kalyaan A, Pinilla P, Krijt S et al. (2023) The Effect of Dust Evolution and Traps on Inner Disk Water Enrichment. *arXiv e-prints* arXiv:2307.01789
- Kama M, Folsom CP, Pinilla P (2015) Fingerprints of giant planets in the photospheres of Herbig stars. *A&A*582:L10
- Kama M, Shorttle O, Jermyn AS et al. (2019) Abundant Refractory Sulfur in Protoplanetary Disks. *ApJ*885(2):114
- Kataoka A, Tanaka H, Okuzumi S, Wada K (2013) Fluffy dust forms icy planetesimals by static compression. *A&A*557:L4
- Kataoka A, Tsukagoshi T, Momose M et al. (2016) Submillimeter Polarization Observation of the Protoplanetary Disk around HD 142527. *ApJ*831(2):L12
- Kataoka A, Tsukagoshi T, Pohl A et al. (2017) The Evidence of Radio Polarization Induced by the Radiative Grain Alignment and Self-scattering of Dust Grains in a Protoplanetary Disk. *ApJ*844(1):L5
- Kenyon SJ, Hartmann L (1987) Spectral Energy Distributions of T Tauri Stars: Disk Flaring and Limits on Accretion. *ApJ*323:714
- Kepler M, Benisty M, Müller A et al. (2018) Discovery of a planetary-mass companion within the gap of the transition disk around PDS 70. *A&A*617:A44

- Klahr HH Henning T (1997) Particle-Trapping Eddies in Protoplanetary Accretion Disks. *Icarus* 128:213–229
- Kluska J, Berger JP, Malbet F et al. (2020) A family portrait of disk inner rims around Herbig Ae/Be stars. Hunting for warps, rings, self shadowing, and misalignments in the inner astronomical units. *A&A*636:A116
- Kratter K Lodato G (2016) Gravitational Instabilities in Circumstellar Disks. *ARA&A*54:271–311
- Kurtovic NT, Pinilla P, Long F et al. (2021) Size and structures of disks around very low mass stars in the Taurus star-forming region. *A&A*645:A139
- Kutra T, Wu Y Qian Y (2021) Super-Earths and Sub-Neptunes Are Insensitive to Stellar Metallicity. *AJ*162(2):69
- Lambrechts M, Johansen A Morbidelli A (2014) Separating gas-giant and ice-giant planets by halting pebble accretion. *A&A*572:A35
- Lambrechts M, Morbidelli A, Jacobson SA et al. (2019) Formation of planetary systems by pebble accretion and migration. How the radial pebble flux determines a terrestrial-planet or super-Earth growth mode. *A&A*627:A83
- Law CJ, Loomis RA, Teague R et al. (2021) Molecules with ALMA at Planet-forming Scales (MAPS). III. Characteristics of Radial Chemical Substructures. *ApJS*257(1):3
- Lazareff B, Berger JP, Kluska J et al. (2017) Structure of Herbig Ae/Be disks at the milliarcsecond scale. A statistical survey in the H band using PIONIER-VLTI. *A&A*599:A85
- Lee CF, Li ZY Turner NJ (2020) Spiral structures in an embedded protostellar disk driven by envelope accretion. *Nature Astronomy* 4:142–146
- Lesur G, Ercolano B, Flock M et al. (2022) Hydro-, Magneto-hydro-, and Dust-Gas Dynamics of Protoplanetary Disks. arXiv e-prints arXiv:2203.09821
- Liu Y, Dipierro G, Ragusa E et al. (2019) Ring structure in the MWC 480 disk revealed by ALMA. *A&A*622:A75
- Lodato G, Dipierro G, Ragusa E et al. (2019) The newborn planet population emerging from ring-like structures in discs. *MNRAS*486(1):453–461
- Long F, Pinilla P, Herczeg GJ et al. (2018) Gaps and Rings in an ALMA Survey of Disks in the Taurus Star-forming Region. *ApJ*869(1):17
- Long F, Herczeg GJ, Harsono D et al. (2019) Compact Disks in a High-resolution ALMA Survey of Dust Structures in the Taurus Molecular Cloud. *ApJ*882(1):49
- Macías E, Guerra-Alvarado O, Carrasco-González C et al. (2021) Characterizing the dust content of disk substructures in TW Hydrae. *A&A*648:A33
- Manara CF, Rosotti G, Testi L et al. (2016) Evidence for a correlation between mass accretion rates onto young stars and the mass of their protoplanetary disks. *A&A*591:L3
- Manara CF, Morbidelli A Guillot T (2018) Why do protoplanetary disks appear not massive enough to form the known exoplanet population? *A&A*618:L3
- Manara CF, Natta A, Rosotti GP et al. (2020) X-shooter survey of disk accretion in Upper Scorpius. I. Very high accretion rates at age \lesssim 5 Myr. *A&A*639:A58
- Manara CF, Ansdell M, Rosotti GP et al. (2022) Demographics of young stars and their protoplanetary disks: lessons learned on disk evolution and its connection to planet formation. arXiv e-prints arXiv:2203.09930
- Marino S (2022) Planetesimal/Debris discs. arXiv e-prints arXiv:2202.03053
- Maucó K, Olofsson J, Canovas H et al. (2020) NaCo polarimetric observations of Sz 91 transitional disc: a remarkable case of dust filtering. *MNRAS*492(2):1531–1542
- Menu J, van Boekel R, Henning T et al. (2015) The structure of disks around intermediate-mass young stars from mid-infrared interferometry. Evidence for a population of group II disks with gaps. *A&A*581:A107
- Meshkat T, Mawet D, Bryan ML et al. (2017) A Direct Imaging Survey of Spitzer-detected Debris Disks: Occurrence of Giant Planets in Dusty Systems. *AJ*154(6):245
- Michel A, van der Marel N Matthews BC (2021) Bridging the Gap between Protoplanetary and Debris Disks: Separate Evolution of Millimeter and Micrometer-sized Dust. *ApJ*921(1):72
- Michel A, Sadavoy SI, Sheehan PD, Looney LW Cox EG (2022) A Millimeter-multipavelength Continuum Study of VLA 1623 West. *ApJ*937(2):104

- Miller E, Marino S, Stammler SM et al. (2021) The formation of wide exoKuiper belts from migrating dust traps. *MNRAS*508(4):5638–5656
- Miotello A, Kamp I, Birnstiel T, Cleeves LI, Kataoka A (2022) Setting the Stage for Planet Formation: Measurements and Implications of the Fundamental Disk Properties. arXiv e-prints arXiv:2203.09818
- Mulders GD (2018) Planet Populations as a Function of Stellar Properties, Springer, p 153. DOI 10.1007/978-3-319-55333-7_153
- Mulders GD, Drazkowska J, van der Marel N, Ciesla FJ, Pascucci I (2021a) Why Do M Dwarfs Have More Transiting Planets? *ApJ*920(1):L1
- Mulders GD, Pascucci I, Ciesla FJ, Fernandes RB (2021b) The Mass Budgets and Spatial Scales of Exoplanet Systems and Protoplanetary Disks. *ApJ*920(2):66
- Musiolik G, Wurm G (2019) Contacts of Water Ice in Protoplanetary Disks—Laboratory Experiments. *ApJ*873(1):58
- Musiolik G, Teiser J, Jankowski T, Wurm G (2016) Ice Grain Collisions in Comparison: CO₂, H₂O, and Their Mixtures. *ApJ*827(1):63
- Najita JR, Kenyon SJ, Bromley BC (2022) From Pebbles and Planetesimals to Planets and Dust: The Protoplanetary Disk-Debris Disk Connection. *ApJ*925(1):45
- Öberg KI, Guzmán VV, Walsh C et al. (2021) Molecules with ALMA at Planet-forming Scales (MAPS). I. Program Overview and Highlights. *ApJS*257(1):1
- Ohashi N, Tobin JJ, Jørgensen JK et al. (2023) Early Planet Formation in Embedded Disks (eDisk). I. Overview of the Program and First Results. *ApJ*951(1):8
- Owen JE (2020) Snow lines can be thermally unstable. *MNRAS*495(3):3160–3174
- Owen JE, Ercolano B, Clarke CJ, Alexander RD (2010) Radiation-hydrodynamic models of X-ray and EUV photoevaporating protoplanetary discs. *MNRAS*401(3):1415–1428
- Pérez LM, Isella A, Carpenter JM, Chandler CJ (2014) Large-scale Asymmetries in the Transitional Disks of SAO 206462 and SR 21. *ApJ*783:L13
- Pérez LM, Chandler CJ, Isella A et al. (2015) Grain Growth in the Circumstellar Disks of the Young Stars CY Tau and DoAr 25. *ApJ*813(1):41
- Pérez LM, Carpenter JM, Andrews SM et al. (2016) Spiral density waves in a young protoplanetary disk. *Science* 353:1519–1521
- Pérez S, Casassus S, Benítez-Llambay P (2018) Observability of planet-disc interactions in CO kinematics. *MNRAS*480:L12–L17
- Pérez S, Casassus S, Hales A et al. (2019) Long baseline observations of HD100546 with ALMA: a possible circumplanetary disk detected in dust continuum and gas kinematics. arXiv e-prints arXiv:1906.06305
- Pfalzner S, Dehghani S, Michel A (2022) Most Planets Might Have More than 5 Myr of Time to Form. *ApJ*939(1):L10
- Picogna G, Ercolano B, Owen JE, Weber ML (2019) The dispersal of protoplanetary discs - I. A new generation of X-ray photoevaporation models. *MNRAS*487(1):691–701
- Pinilla P, Benisty M, Birnstiel T (2012a) Ring shaped dust accumulation in transition disks. *A&A*545:A81
- Pinilla P, Benisty M, Birnstiel T (2012b) Ring shaped dust accumulation in transition disks. *A&A*545:A81
- Pinilla P, Birnstiel T, Benisty M et al. (2013) Explaining millimeter-sized particles in brown dwarf disks. *A&A*554:A95
- Pinilla P, Benisty M, Birnstiel T et al. (2014) Millimetre spectral indices of transition disks and their relation to the cavity radius. *A&A*564:A51
- Pinilla P, de Juan Ovelar M, Ataiee S et al. (2015) Gas and dust structures in protoplanetary disks hosting multiple planets. *A&A*573:A9
- Pinilla P, Pohl A, Stammler SM, Birnstiel T (2017) Dust Density Distribution and Imaging Analysis of Different Ice Lines in Protoplanetary Disks. *ApJ*845(1):68
- Pinilla P, Tazzari M, Pascucci I et al. (2018) Homogeneous Analysis of the Dust Morphology of Transition Disks Observed with ALMA: Investigating Dust Trapping and the Origin of the Cavities. *ApJ*859(1):32

- Pinilla P, Pascucci I, Marino S (2020) Hints on the origins of particle traps in protoplanetary disks given by the $M_{dust} - M_*$ relation. *A&A*635:A105
- Pinilla P, Garufi A, Gárate M (2022) Efficient dust radial drift around young intermediate-mass stars. *A&A*662:L8
- Pinte C, Price DJ, Ménard F et al. (2018) Kinematic Evidence for an Embedded Protoplanet in a Circumstellar Disk. *ApJ*860:L13
- Pinte C, Teague R, Flaherty K et al. (2022) Kinematic Structures in Planet-Forming Disks. arXiv e-prints arXiv:2203.09528
- Pohl A, Kataoka A, Pinilla P et al. (2016) Investigating dust trapping in transition disks with millimeter-wave polarization. *A&A*593:A12
- Pringle JE (1981) Accretion discs in astrophysics. *ARA&A*19:137–162
- Qi C, Öberg KI, Wilner DJ (2013) H_2CO and N_2H^+ in Protoplanetary Disks: Evidence for a CO-ice Regulated Chemistry. *ApJ*765:34
- Qi C, Öberg KI, Espaillat CC et al. (2019) Probing CO and N_2 Snow Surfaces in Protoplanetary Disks with N_2H^+ Emission. *ApJ*882(2):160
- Rab C, Kamp I, Dominik C et al. (2020) Interpreting high spatial resolution line observations of planet-forming disks with gaps and rings: the case of HD 163296. *A&A*642:A165
- Ragusa E, Dipierro G, Lodato G, Laibe G, Price DJ (2017) On the origin of horseshoes in transitional discs. *MNRAS*464:1449–1455
- Rao R, Girart JM, Lai SP, Marrone DP (2014) Detection of a Magnetized Disk around a Very Young Protostar. *ApJ*780(1):L6
- Ribas Á, Macías E, Weber P et al. (2023) The ALMA view of MP Mus (PDS 66): A protoplanetary disk with no visible gaps down to 4 au scales. *A&A*673:A77
- Ricci L, Testi L, Natta A et al. (2010) Dust properties of protoplanetary disks in the Taurus-Auriga star forming region from millimeter wavelengths. *A&A*512:A15
- Rosotti GP (2023) Empirical constraints on turbulence in proto-planetary discs. *New A Rev*96:101674
- Rosotti GP, Juhasz A, Booth RA, Clarke CJ (2016) The minimum mass of detectable planets in protoplanetary discs and the derivation of planetary masses from high-resolution observations. *MNRAS*459(3):2790–2805
- Rosotti GP, Benisty M, Juhász A et al. (2019) Spiral arms in the proto-planetary disc HD100453 detected with ALMA: evidence for binary-disc interaction and a vertical temperature gradient. *MNRAS*sp 2689
- Segura-Cox DM, Schmiedeke A, Pineda JE et al. (2020) Four annular structures in a protostellar disk less than 500,000 years old. *Nature*586(7828):228–231
- Sellek AD, Booth RA, Clarke CJ (2020) A dusty origin for the correlation between protoplanetary disc accretion rates and dust masses. *MNRAS*498(2):2845–2863
- Shakura NI, Sunyaev RA (1973) Black holes in binary systems. Observational appearance. *A&A*24:337–355
- Sheehan PD, Eisner JA (2017) WL 17: A Young Embedded Transition Disk. *ApJ*840(2):L12
- Sheehan PD, Eisner JA (2018) Multiple Gaps in the Disk of the Class I Protostar GY 91. *ApJ*857(1):18
- Sheehan PD, Tobin JJ, Federman S, Megeath ST, Looney LW (2020) The VLA/ALMA Nascent Disk and Multiplicity (VANDAM) Survey of Orion Protostars. III. Substructures in Protostellar Disks. *ApJ*902(2):141
- Sibthorpe B, Kennedy GM, Wyatt MC et al. (2018) Analysis of the Herschel DEBRIS Sun-like star sample. *MNRAS*475(3):3046–3064
- Stadler J, Benisty M, Izquierdo A et al. (2023) A kinematically detected planet candidate in a transition disk. *A&A*670:L1
- Stammler SM, Birnstiel T (2022) DustPy: A Python Package for Dust Evolution in Protoplanetary Disks. *ApJ*935(1):35
- Stammler SM, Drazkowska J, Birnstiel T et al. (2019) The DSHARP Rings: Evidence of Ongoing Planetesimal Formation? *ApJ*884(1):L5

- Stapper L, Hogerheijde MR, van Dishoeck EF, Mentel R (2021) The mass and size of Herbig disks as seen by ALMA. arXiv e-prints arXiv:2112.03297
- Steinpilz T, Teiser J, Wurm G (2019) Sticking Properties of Silicates in Planetesimal Formation Revisited. *ApJ*874(1):60
- Tabone B, Bettoni G, van Dishoeck EF et al. (2023) A rich hydrocarbon chemistry and high C to O ratio in the inner disk around a very low-mass star. *Nature Astronomy*
- Tang YW, Guilloteau S, Dutrey A et al. (2017) Planet Formation in AB Aurigae: Imaging of the Inner Gaseous Spirals Observed inside the Dust Cavity. *ApJ*840(1):32
- Tang YW, Dutrey A, Koch PM et al. (2023) Polarization in the GG Tau Ring-Confronting Dust Self-scattering, Dust Mechanical and Magnetic Alignment, Spirals, and Dust Grain Drift. *ApJ*947(1):L5
- Tazzari M, Clarke CJ, Testi L et al. (2021a) Multiwavelength continuum sizes of protoplanetary discs: scaling relations and implications for grain growth and radial drift. *MNRAS*506(2):2804–2823
- Tazzari M, Testi L, Natta A et al. (2021b) The first ALMA survey of protoplanetary discs at 3 mm: demographics of grain growth in the Lupus region. *MNRAS*506(4):5117–5128
- Teague R, Bae J, Bergin EA, Birnstiel T, Foreman-Mackey D (2018) A Kinematical Detection of Two Embedded Jupiter-mass Planets in HD 163296. *ApJ*860:L12
- Teague R, Bae J, Huang J, Bergin EA (2019) Spiral Structure in the Gas Disk of TW Hya. *ApJ*884(2):L56
- Testi L, Natta A, Shepherd DS, Wilner DJ (2001) Constraints on Properties of the Protoplanetary Disks around UX Orionis and CQ Tauri. *ApJ*554(2):1087–1094
- Tobin JJ, Sheehan PD, Megeath ST et al. (2020) The VLA/ALMA Nascent Disk and Multiplicity (VANDAM) Survey of Orion Protostars. II. A Statistical Characterization of Class 0 and Class I Protostellar Disks. *ApJ*890(2):130
- Tripathi A, Andrews SM, Birnstiel T, Wilner DJ (2017) A millimeter Continuum Size-Luminosity Relationship for Protoplanetary Disks. *ApJ*845:44
- Tychoniec Ł, Manara CF, Rosotti GP et al. (2020) Dust masses of young disks: constraining the initial solid reservoir for planet formation. *A&A*640:A19
- Ubeira Gabellini MG, Miotello A, Facchini S et al. (2019) A dust and gas cavity in the disc around CQ Tau revealed by ALMA. *MNRAS*486(4):4638–4654
- Uribe AL, Klahr H, Flock M, Henning T (2011) Three-dimensional Magnetohydrodynamic Simulations of Planet Migration in Turbulent Stratified Disks. *ApJ*736(2):85
- van der Marel N (2023) Transition disks: the observational revolution from SEDs to imaging. *European Physical Journal Plus* 138(3):225
- van der Marel N, Mulders GD (2021) A Stellar Mass Dependence of Structured Disks: A Possible Link with Exoplanet Demographics. *AJ*162(1):28
- van der Marel N, van Dishoeck EF, Bruderer S et al. (2013) A Major Asymmetric Dust Trap in a Transition Disk. *Science* 340:1199–1202
- van der Marel N, Pinilla P, Tobin J et al. (2015) A Concentration of Centimeter-sized Grains in the Ophiuchus IRS 48 Dust Trap. *ApJ*810(1):L7
- van der Marel N, van Dishoeck EF, Bruderer S et al. (2016) Resolved gas cavities in transitional disks inferred from CO isotopologs with ALMA. *A&A*585:A58
- van der Marel N, Williams JP, Ansdell M et al. (2018) New Insights into the Nature of Transition Disks from a Complete Disk Survey of the Lupus Star-forming Region. *ApJ*854:177
- van der Marel N, Dong R, di Francesco J, Williams JP, Tobin J (2019) Protoplanetary Disk Rings and Gaps across Ages and Luminosities. *ApJ*872(1):112
- van der Marel N, Birnstiel T, Garufi A et al. (2021a) On the Diversity of Asymmetries in Gapped Protoplanetary Disks. *AJ*161(1):33
- van der Marel N, Booth AS, Leemker M, van Dishoeck EF, Ohashi S (2021b) A major asymmetric ice trap in a planet-forming disk. I. Formaldehyde and methanol. *A&A*651:L5
- van der Marel N, Williams JP, Picogna G et al. (2022) High-resolution ALMA observations of transition disk candidates in Lupus. arXiv e-prints arXiv:2204.08225

- Varga J, Hogerheijde M, van Boekel R et al. (2021) The asymmetric inner disk of the Herbig Ae star HD 163296 in the eyes of VLTI/MATISSE: evidence for a vortex? *A&A*647:A56
- Villeneuve M, Ménard F, Dent WRF et al. (2020) Observations of edge-on protoplanetary disks with ALMA. I. Results from continuum data. *A&A*642:A164
- Villeneuve M, Stapelfeldt KR, Duchêne G et al. (2022) A Highly Settled Disk around Oph163131. *ApJ*930(1):11
- Villeneuve M, Podio L, Duchêne G et al. (2023) Modest Dust Settling in the IRAS04302+2247 Class I Protoplanetary Disk. *ApJ*946(2):70
- Wada K, Tanaka H, Suyama T, Kimura H Yamamoto T (2011) The Rebound Condition of Dust Aggregates Revealed by Numerical Simulation of Their Collisions. *ApJ*737(1):36
- Weidenschilling SJ (1977) Aerodynamics of solid bodies in the solar nebula. *MNRAS*180:57–70
- Williams JP, Cieza L, Hales A et al. (2019) The Ophiuchus Disk Survey Employing ALMA (ODISEA): Disk Dust Mass Distributions across Protostellar Evolutionary Classes. *ApJ*, in press
- Wyatt MC, Panić O, Kennedy GM Matrà L (2015) Five steps in the evolution from protoplanetary to debris disk. *Ap&SS*357:103
- Youdin AN Goodman J (2005) Streaming Instabilities in Protoplanetary Disks. *ApJ*620(1):459–469
- Youdin AN Lithwick Y (2007) Particle stirring in turbulent gas disks: Including orbital oscillations. *Icarus*192(2):588–604
- Zhang K, Bergin EA, Blake GA et al. (2016) On the Commonality of 10-30 AU Sized Axisymmetric Dust Structures in Protoplanetary Disks. *ApJ*818(1):L16
- Zhang S, Zhu Z, Huang J et al. (2018) The Disk Substructures at High Angular Resolution Project (DSHARP). VII. The Planet-Disk Interactions Interpretation. *ApJ*869(2):L47
- Zhu W Wu Y (2018) The Super Earth-Cold Jupiter Relations. *AJ*156(3):92
- Zhu Z, Nelson RP, Hartmann L, Espaillat C Calvet N (2011) Transitional and Pre-transitional Disks: Gap Opening by Multiple Planets? *ApJ*729(1):47
- Zhu Z, Andrews SM Isella A (2018) On the radio detectability of circumplanetary discs. *MNRAS*479(2):1850–1865
- Zormpas A, Birnstiel T, Rosotti GP Andrews SM (2022) A large population study of protoplanetary disks: Explaining the millimeter size-luminosity relation with or without sub-structure. arXiv e-prints arXiv:2202.01241